Highlights

- Hypermineralised vertebrate apatite yields $\delta^{18}O$ values comparable to conodonts
- Dentine yields lower and more heterogeneous $\delta^{18}O$ values than hypermineralised tissues
- GIRMS of bulk vertebrate fossils produced $\delta^{18}O$ values depleted in ^{18}O by 2-4 ‰
- Dentine O-isotope ratios are likely modified by microbes and fluid interaction
- Vertebrate microfossils offer a potential substitute for conodonts in O-isotope studies

Assessing the fidelity of marine vertebrate microfossil $\delta^{18}O$ signatures and their potential for palaeo-ecological and -climatic reconstructions

Brett Roelofs [a,*], Milo Barham [a,b], John Cliff [c], Michael Joachimski [d], Laure Martin [e] and Kate Trinajstic [b,f]

[a]Department of Applied Geology, Curtin University, GPO Box U1987, Perth, WA 6845, Australia

[b]The Institute for Geoscience Research (TIGeR), Department of Applied Geology, Curtin University, GPO Box U1987, Perth, Australia

[c]Environmental Molecular Science Laboratory (EMSL), Pacific Northwest National Laboratory, P.O. Box 999 Richland, WA 99352, USA.

[d]GeoZentrum Nordbayern, University of Erlangen-Nuremberg, Schlossgarten 5, 91054 Erlangen, Germany

[e]Centre for Microscopy, Characterisation and Analysis (CMCA), The University of Western Australia, Perth, WA 6009, Australia

[f]Department of Environment and Agriculture, Curtin University, GPO Box U1987, Perth, WA 6845, Australia

ABSTRACT

Conodont biogenic apatite has become a preferred analytical target for oxygen isotope studies investigating ocean temperature and palaeoclimate changes in the Palaeozoic. Despite the growing application in geochemically-based palaeoenvironmental reconstructions, the paucity or absence of conodont fossils in certain facies necessitates greater flexibility in selection of robust oxygen-bearing compounds for analysis. Vertebrate microfossils (teeth, dermal denticles, spines) offer a potential substitute for conodonts from the middle Palaeozoic. Vertebrate bioapatite is particularly advantageous given a fossil record extending to the present with representatives across freshwater to fully marine environments, thus widening the scope of oxygen isotope studies on bioapatite. However, significant tissue heterogeneity within vertebrates and differential susceptibility of these tissues to diagenetic alteration have been raised as potential problems affecting the reliability of the oxygen isotope ratios as palaeoclimatic proxies. Well-preserved vertebrate microfossils and co-occurring conodont fossils from the Upper Devonian and Lower Carboniferous of the Lennard Shelf, Canning Basin, Western Australia, were analysed using bulk (gas isotope ratio mass spectrometry, GIRMS) and in-situ (secondary ion mass spectrometry, SIMS) methodologies, with the latter technique allowing investigation of specific tissues within vertebrate elements. The $\delta^{18}O_{conodont}$ results may be interpreted in terms of palaeolatitudinally and environmentally sensible palaeo-salinity and -temperature and provide a baseline standard for comparison against vertebrate microfossil $\delta^{18}O$ values. Despite an absence of obvious diagenetic modification, GIRMS of vertebrate denticles yielded $\delta^{18}O$ values depleted in ^{18}O by 2-4 ‰ relative to co-occurring conodonts. SIMS analysis of dentine tissues exhibited significant heterogeneity, while hypermineralised tissues in

both scales and teeth produced $\delta^{18}O$ values comparable with those of associated conodonts. The susceptibility of permeable phosphatic fossil tissues to microbial activity, fluid interaction and introduction of mineral precipitates post-formation is demonstrated in the dentine of vertebrate microfossils, which showed significant heterogeneity and consistent depletion in ^{18}O relative to conodonts. The hypermineralised tissues present in both teeth and scales appear resistant to many diagenetic processes and indicate potential for palaeoclimatic reconstructions and palaeoecological investigations.

Keywords: SIMS; GIRMS; apatite; temperature; histology; oxygen-isotopes

1. Introduction

The Palaeozoic marine oxygen isotope record is punctuated by a series of excursions and perturbations reflecting climatic events that are often associated with significant biological reorganisations (e.g. Brand, 1989; Gruszcyński et al., 1989; Caplan and Bustin, 1999; Veizer et al., 1999; Jeppsson et al., 2002; Joachimski and Buggisch, 2002; Kaiser et al., 2006; Trotter, 2008; Schobben et al., 2015). Fluctuations in the oxygen isotope record have been elicited from analysis of marine organisms with the ability to precipitate mineralised tissues in isotopic equilibrium with the ambient water. The shells of Palaeozoic low-Mg calcite brachiopod taxa have been commonly used (Popp et al., 1986; Veizer et al., 1986, 1997; Brand, 1989, 2004; Carpenter et al., 1991; Hays and Grossman, 1991; Wadleigh et al., 1992; Azmy et al., 1996; Mii et al., 1997, 1999; Van Geldern et al., 2006; Korte et al., 2008) due to their relative abundance, ease of sampling and the relative resistance of low-Mg calcite, compared to aragonite or high-Mg calcite, to post-mortem

modification. Recent work however has shown that even low-Mg calcite is highly susceptible to diagenesis over time (Cummins et al., 2014). This issue is compounded by imperfect screening methods for the identification of recrystallised calcite, which may cause resetting of oxygen isotope values (e.g. Wenzel et al., 2000). In addition, O-isotope heterogeneity has been identified in a number of brachiopod shells, indicating fractionation is occurring during the formation of these hard tissues (e.g. Auclair et al., 2003; Yamamoto et al., 2011; Rollion-Bard et al., 2016). The typically sessile ecology of brachiopods also means that each analysis must be independently considered in the context of the specific temperature and chemistry of the water depth it inhabited. Consequently, this limits the comparison of oxygen isotope signatures to brachiopod taxa occupying similar ecological niches (Popp et al., 1986; James et al., 1997).

Bioapatite offers a more physically and chemically resistant oxygen-bearing alternative to brachiopod calcite due to a greater mineral hardness and stability of the P-O bond in PO_4^{3-} (e.g., Grimes et al., 2003; Joachimski et al., 2004). The mineralised feeding elements of conodonts (Lindström, 1974; Dzik, 1991; Goudemand et al., 2011) comprise a relatively homogenous chemical composition ($Ca_5Na_{0.13}(PO_4)_{3.01}(CO_3)_{0.16}F_{0.73}(H2O)_{0.85}$, Pietzner et al., 1986) and have become increasingly used in oxygen isotope studies. Despite a non-ubiquitous internal structure among all taxa (Donoghue, 1998; Trotter et al., 2007), the mineralised element crowns typically comprise a translucent finely crystallised hyaline tissue and an inner albid tissue (Lindström, 1964; Pietzner et al., 1968; Barnes et al. 1973; Donoghue, 1998; Trotter et al., 2007; Jones et al., 2012). Analysis of their hypermineralised tissues indicates conodont elements offer greater uniformity in $\delta^{18}O$ values in comparison to those obtained from brachiopod calcite (e.g. Wallace

and Elrick, 2014). Consistent oxygen isotope signatures have been observed between conodont genera belonging to different biofacies in the Late Devonian (Joachimski et al., 2009) and Carboniferous (Joachimski and Lambert, 2015), supporting a shared near sea-surface marine habitat and free swimming lifestyle, as suggested from their biology (e.g. Gabbott et al., 1995). This observation may be dependent on location, time period and genera analysed, as recent work on Ordovician (Quinton and Macleod, 2014), Permian (Joachimski et al., 2012) and Triassic (Trotter et al., 2015) conodonts has shown discernible differences in $\delta^{18}O$ values between some genera. Despite some taxon-specific discrepancies in $\delta^{18}O$, correlatable oxygen isotope ratios have proven useful in wider geographical comparisons (e.g. Joachimski et al., 2009).

The biostratigraphic utility and widespread distribution and abundance of conodont elements in many marine deposits has facilitated the development of a temporally resolved isotope record spanning many significant faunal reorganisations associated with climatic perturbations from the Ordovician (Trotter et al., 2008) to the Triassic (Joachimski et al., 2009; Rigo et al., 2012; Sun et al., 2012; Trotter et al., 2015). However, conodont fossils are not ubiquitous in all facies, limiting their potential as a sea surface temperature proxy in many regions. Even where present, a paucity of conodont elements can preclude preferred single genera sample analysis and fine resolution sampling due to minimum sample mass requirements in standard analytical methodologies. As a consequence of these limitations, other common, diagenetically resistant oxygen-bearing compounds must be identified to expand accurate palaeoenvironmental interpretations across different temporal intervals and depositional settings.

We studied a range of vertebrate microfossil elements using GIRMS to determine the stability of biogenic phosphate over geological timescales, as well as

the degree to which ecology and diagenesis influence oxygen isotope ratios in different vertebrate microfossil remains. Secondary ion mass spectrometry (SIMS) analysis was applied to test whether all vertebrate microfossil tissues are equally prone or resistant to alteration of their O-isotopic ratios. In order to establish the validity of vertebrate microfossil $\delta^{18}O$ signatures and their potential use as palaeoclimatic indicators, the oxygen isotope ratios of vertebrate microfossils were compared with those of co-occurring conodonts. Both GIRMS and SIMS analyses were undertaken on Frasnian (Upper Devonian) conodont samples as well as multiple Famennian (Upper Devonian) and Tournaisian (Lower Carboniferous) conodont and vertebrate remains to i) document any potential discrepancies between the two methods and; to ii) identify potential causes of disruption of primary oxygen isotope signatures in different vertebrate tissues.

2. Background

2.1. Vertebrate microfossil histology

Marine vertebrate microfossils (typically less than 5 mm in size) most commonly comprise teeth, scales and fin spines. The hard tissues of vertebrates are highly heterogeneous, consisting of three broad types; bone, dentine and enamel. These tissues are differentiated by the levels of mineralisation and organic matter content. Bone comprises a 50-70 % mineralised component with 20-40 % organic matter and 5-10 % water (Clarke, 2005). Dentine is approximately 70 % mineralised with 20-24 % protein and 6-10 % water, whereas enamel is highly mineralized (96 %) with only 1 % protein and approximately 3 % water, which is present on or between the hydroxyapatite crystals (Stack, 1955; Pasteris et al., 2008; Goldberg et al., 2012; Hand and Frank, 2014). The O-hosting sites within biogenic apatite also

differ significantly between vertebrate hard tissues (Pasteris et al., 2008). Bone and dentine comprise 6 and 5 wt % CO_3^{2-} respectively, with only ~3.5 wt % present in enamel (LeGeros and LeGeros, 1983; Cerling and Sharp, 1996). This low CO_3^{2-} concentration compared to dentine and bone, in addition to a high degree of mineralisation (>80 wt %, Li, 2013), makes the hypermineralised tissues (enamel, enameloid, ganoine and acrodin) present in vertebrate teeth and scales more resistant to physical and chemical alteration. Detailed information on tooth and scale histology of analysed taxa is provided in the supplementary material (A1-VH).

2.2. Application of vertebrate tissues in Palaeozoic oxygen isotope studies

Oxygen isotopes of vertebrate bioapatite tissues have been previously used to determine palaeoenvironmental conditions in the Palaeozoic (Kolodny and Luz, 1991; Barham, 2012a; Fischer et al., 2013) and Mesozoic (Kolodny and Raab, 1988; Kolodny and Luz, 1991; Lécuyer et al., 1993; Pucéat et al., 2003; Billon-Bruyat et al., 2005; Fischer et al., 2012). Applying gas isotope ratio mass spectrometry (GIRMS) to Palaeozoic vertebrate fossils, however, has produced inconsistent results when whole fossils are used. Analysis of Upper Devonian actinopterygian teeth (Joachimski and Buggisch, 2002) initially suggested that original oxygen isotope ratios were preserved in the tooth apatite. Other works however, have revealed that Palaeozoic vertebrate teeth and dermal denticles are typically depleted in ^{18}O (relative to conodont elements) between 2.4 and 2.9 ‰ (Barham et al., 2012a; Žigaite et al., 2010). This has led to the suggestion that vertebrate microfossil elements are susceptible to diagenetic affects and thus may not preserve original isotopic signatures (Barham et al., 2012a). However, given that secondary alteration

may be tissue-specific or screened and subsequently avoided, the potential still exists for the geochemistry of these fossils to serve as a palaeoclimatic archive.

3. Materials and methods

3.1. Sample collection, processing and imaging

Upper Devonian vertebrate microfossils are common in the distal slope facies of the Virgin Hills Formation (late Frasnian - middle Famennian; Fig. 1; Playford et al., 2009; Trinajstic and George, 2009; Trinajstic et al., 2014; Roelofs et al., 2015) and in the conodont-poor facies of the Fairfield Group (Upper Devonian-Lower Carboniferous) (Roelofs et al., 2016; Thomas, 1957, 1959). Twenty kilogram samples were collected from single beds at Horse Spring (18°11′41″ S, 126°01′69″ E) (sample prefix VHS), Oscar Hill (18°04'07" S, 125°26'41" E) (sample prefixes OH, Si) and Laurel Downs (18°01'37" S, 125°18'43" E) (sample prefixes 1984, CCA, MT and MTM) (Fig. 1) and processed using a buffered 10 % acetic acid solution (following the methodology of Jeppsson et al., 1999). The rock samples were disaggregated as whole rocks with rinsing occurring every 24-48 h, depending on the degree of disaggregation. This process was repeated, with fresh 10 % buffered acetic acid, until the rocks had been sufficiently broken down to allow for the removal of isolated fossils. Residues were rinsed and sieved (0.125 mm sieve) to further separate microfossils before picking the >0.125 mm fraction under a Nikon stereomicroscope. Detailed examination of microfossils was performed using a Hitachi TM-3030 desktop Scanning Electron Microscope (SEM) at Curtin University with accelerating voltages ranging from 5-15 kV and variable pressures. Eight larger holocephalan teeth (>10 mm mesio-distally) were recovered directly from the disaggregated rock residues. A single tooth (MTM1-H9) was exposed from

200 the rock sample along its labial face and extracted prior to processing. Additional
201 imaging of analysed specimens was performed using a Leica stereomicroscope
202 camera at the Western Australian Museum.

203 Horse Spring samples yielded 200 conodont elements corresponding to
204 Conodont Zone (CZ) 11 (Frasnian; Klapper, 1989). Conodont yields from Oscar Hill
205 samples taken for this study yielded mainly undiagnostic elements with a single long
206 ranging Famennian conodont *Spathognathodus aciedentatus* recovered. Previous
207 sampling by Nicoll and Druce (1979) indicated a latest Famennian age (*praesulcata*
208 Conodont Zone) for outcrop at Oscar Hill. Tournaisian rock samples (Table 2) were
209 collected from a bioclastic limestone bed of the Laurel Formation (sample number
210 1984-04), exposed approximately 35 km northwest of the town of Fitzroy Crossing
211 (Fig. 1). A Tournaisian age is supported by the presence of the conodont taxa
212 *Clydagnathus cavusformis* and *Bispathodus aculeatus*, and is consistent with
213 previous age determinations (Druce and Radke, 1979; Nicoll and Druce, 1979). A
214 refinement of early Tournaisian for the sampled area is indicated by the overlap of
215 shark species *Thrinacodus ferox*, *Protacrodus aequalis* and *Protacrodus* sp. 1
216 (Roelofs et al., 2016).

217

218 *3.2. Analytical methodology*

219 The GIRMS method has conventionally been used to accurately determine
220 the $\delta^{18}O$ values of pooled apatite fossils through the analysis of chemically purified
221 Ag_3PO_4. To obtain ~1 mg of fossil material required for replicate analyses, samples
222 comprising multiple vertebrate microfossil elements, or single elements comprising
223 multiple tissue types, are often required. The incorporation of different fossil tissues
224 within analyses reduces data confidence as tissue geochemistry is differently affected

by biological processes including organism physiology (e.g. Thorrold et al. 1997), post-mortem microbial activity (Blake et al., 1997, 1998; Zazzo et al., 2003) as well as physico-chemical influences such as diagenesis (e.g. Iacumin et al., 1996).

The use of laser ablation techniques on biogenic phosphate has demonstrated the potential to measure and quantify variation in $\delta^{18}O$ from in-situ tissues (Cerling and Sharp, 1996). Such in-situ techniques minimise potential contamination and alteration of samples during preparation and reduce the required sample size (Brady, 2004). Trotter et al. (2008) later established the use of secondary ion mass spectrometry (SIMS) on biogenic phosphate to elicit reliable $\delta^{18}O$ values from both fossil and modern tissue. This success of this work has been replicated with a particular focus on conodonts, in reconstructing Palaeozoic paleoclimates and paleoceanographies (Rigo et al., 2012; Wheeley et al., 2012; Trotter et al., 2015; Chen et al., 2016). Whether this technique can be applied to Palaeozoic vertebrates and the preservation of $\delta^{18}O$ in highly heterogeneous fossil tissues has not been thoroughly explored. Application of this technique to modern shark teeth (Trotter et al., 2008; Žigaite and Whitehouse, 2014) has shown preservation of original oxygen isotope signatures in hypermineralised tissues as well as heterogeneity and depletion of ^{18}O within the more permeable dentine (Žigaite and Whitehouse, 2014).

Following the approach of Trotter et al. (2008), aliquots of a single large fragment of Durango apatite crystal were used as an oxygen isotope standard for comparison between GIRMS and SIMS methods and published data. It should be noted that recent work by Sun et al. (2016) has highlighted a 4.4 ‰ inter-crystal $\delta^{18}O$ variation between Durango apatite crystals as well as intra-crystal variation that ranged from 0.7-1.8 ‰. To minimise the potential effects of crystal heterogeneity, ion probe spots were concentrated on small areas within small fragments of a single

crystal. Additionally, as this work focuses on intra-fossil variation as well as comparing fossils on the same mount, potential variation between crystal fragments does not significantly alter the conclusions of this work.

3.2.1. GIRMS oxygen isotope analyses

Stable oxygen isotope ratios were determined on conodont and vertebrate microfossil material at the Stable Isotope Laboratory of the University of Erlangen-Nürnberg, Germany, following a modified version of the procedure developed by O'Neil et al. (1994) and described in Joachimski et al. (2009). Conodont, vertebrate microfossil and Durango apatite samples (0.7-2.0 mg) were chemically converted to trisilverphosphate (Ag_3PO_4) and the oxygen isotope ratios of ~0.2 mg sample aliquots were analysed as CO produced in a high temperature conversion elemental analyser (TC−EA) attached on-line to a ThermoFisher Delta V Plus mass spectrometer. Oxygen isotope compositions are reported in δ notation in ‰ relative to Vienna Standard Mean Ocean Water (VSMOW) (Table 1). The analyses were calibrated by performing a two-point calibration (Paul et al., 2007) using NBS 120c (+21.7 ‰) and a commercial Ag_3PO_4 (+9.9 ‰). All standards were calibrated to TU1 (+21.11 ‰) and TU2 (+5.45 ‰; Vennemann et al., 2002). A laboratory standard, as well as NBS 120c were used as control standards and processed together with the samples. Replicate analyses of the international standard NBS 120c and internal laboratory standards were performed between every four unknowns, as well as at the start and end of each measuring day to monitor accuracy and reproducibility. Reproducibility was typically ±0.2 ‰ (1σ). NBS 120c was measured as +21.7 ±0.1 ‰ (1σ, n = 12) VSMOW (within uncertainty reported by Laporte et al., 2009). Most samples were measured in triplicate, with limited Ag_3PO_4 from

samples OH4-C and 1984-C only allowing duplicate and single analyses, respectively.

3.2.2. SIMS oxygen isotope analyses

Conodont and vertebrate microfossils, with fragments of a Durango apatite crystal were mounted on double sided tape attached to standard glass plates. Large holocephalan teeth were cut labio-lingually using a Dremel rotary tool and ground flat with 1200 grit sandpaper prior to mounting on the tape along the smooth surface. Struers EpoFix epoxy resin was used to form standard one-inch round mounts and then polished to expose the desired tissues using successively finer polishing cloths to a 1 μm finish. The mounts were then carefully cleaned with detergent, distilled water and isopropanol in an ultrasonic bath and coated with gold (30 nm in thickness) prior to SIMS analyses.

Oxygen isotope ratios were determined using a Cameca IMS 1280 multi-collector ion microprobe located at the Centre for Microscopy, Characterisation and Analysis (CMCA), University of Western Australia (UWA) in March and November 2014. Analyses were performed with a ca. 2.5 nA Cs^+ beam with a total impact energy of 20 keV rastered on a ca. 20 x 20 μm area on the sample surface. Instrument parameters included a magnification of 130 × between the sample and field aperture (FA), 400 μm contrast aperture (CA), 4000 μm FA, 110 μm entrance slit, 400 μm exit slits, and a 40 eV band pass for the energy slit with a 5 eV gap toward the high energy side. Secondary O^- ions were accelerated to 10 keV and analysed with a mass resolving power of approximately 2200 using dual Faraday Cup detectors. A normal-incidence electron gun was used to provide charge compensation and NMR regulation was employed for magnetic field control.

299 Ten seconds of pre-sputtering was followed by automatic centering of the
300 secondary beam in the FA and CA. Each analysis consisted of 20 four-second cycles,
301 which gave an average internal precision of ±0.2 ‰ (1σ). Analytical sessions were
302 monitored for drift and precision using a bracketing standard (Durango apatite; +9.9
303 ±0.3 ‰, (1σ, n = 9); characterised via GIRMS of three samples analysed in triplicate
304 from the same crystal) for every six sample analyses. Instrumental mass fractionation
305 (IMF) was corrected using Durango apatite following the procedure described in
306 Kita et al. (2009). The spot-to-spot reproducibility (external precision) was typically
307 ±0.3-0.4 ‰ (1σ) on Durango apatite during all of the analytical sessions, except two
308 sessions at ±0.2 ‰ (sample HT2) and ±0.5 ‰ (sample MVM2). Uncertainty on each
309 spot was calculated by propagating the errors on instrumental mass fractionation
310 determination and internal error on each sample data point. The resulting uncertainty
311 was typically between ±0.3 and ±0.6 ‰ (1σ). Raw $^{18}O/^{16}O$ ratios and corrected $\delta^{18}O$
312 (reported relative to VSMOW) are presented in Table 2.
313
314 **4. Results**
315 *4.1. Fossil preservation*
316 Visual inspection (both macro- and microscopic) confirmed conodont
317 elements were well-preserved, showing no evidence of coarsening crystallites,
318 pitting, overgrowths or other visible signs of diagenetic modification (Fig. 2; Nöth,
319 1998). Vertebrate microfossil elements are similarly apparently well-preserved with
320 smooth lustrous surfaces present on the cusps of teeth and dermal denticle crowns. In
321 cross section, the dentine of all teeth was light grey to white in colour with the
322 exception of sample MTM1-H9, which showed a dark grey discolouration around
323 one margin that correlates to the previously exposed labial surface of the tooth.

Reddish coloured staining is present within the basal tissue in sample MTM1-H1, along with calcite cement in some of the pore canals that extend from the cusp surface to the basal tissue.

4.2. GIRMS $\delta^{18}O$ analysis of vertebrate microfossil *elements*

The $\delta^{18}O$ values of Famennian vertebrate microfossils ranged from +16.2-17.1 ‰ (VSMOW) (Table 1) with a mean of +16.7 ‰. The $\delta^{18}O$ values obtained from the Tournaisian vertebrate microfossil samples are more variable than Famennian values, ranging from +15.7 to 19.1 ‰. The largest disparity in $\delta^{18}O$ was measured in the outer cusp tissue of Tournaisian holocephalan teeth (+16.0 to 19.1 ‰, mean of +17.8 ‰; Fig. 3). Similar $\delta^{18}O$ values were obtained from ctenacanthid (+16.0 ‰) and protacrodont (+17.1 ‰) scales from the Famennian. Inter-taxa variation of <1.2 ‰ was found for Tournaisian acanthodian (+17.0 ‰), lungfish (+16.5 ‰), ctenacanthiform (+16.9 ‰), protacrodont (+16.1 and +17.2 ‰) and palaeoniscoid scales (+19.0 ‰) (Table 1). Significant intra-specific disparity in $\delta^{18}O$ values within Tournaisian vertebrate scales was seen between protacrodont scales recording values of +16.1 and +17.2 ‰. The lowest $\delta^{18}O$ values were recorded in Tournaisian palaeoniscoids, with values of +15.7 (radial bone) and +15.9 ‰ (tooth) (Fig. 3). However, $\delta^{18}O$ values of associated palatal teeth were consistently higher at +18.0 ‰ (sample 1984-B) and +18.1 ‰ (sample 1984-H).

4.3. SIMS $\delta^{18}O$ analyses

In-situ oxygen isotope analyses were performed on three late Famennian and two early Tournaisian conodont elements (Table 2). Conodont $\delta^{18}O$ values from averaged spot analyses on three late Famennian S-elements range from +18.7 to 20.8

‰ (Table 2), with an average value of +19.6 ±0.5 ‰. Two to five individual spots were analysed on the blades of the S-elements with a deviation between spots on each element ranging from 0 to +1.0 ‰ (Table 2). Two P_1 elements (*sensu* Purnell et al., 2000) of the early Tournaisian conodont *Clydagnathus cavusformis* produced average $\delta^{18}O$ values of +19.9 ‰ (±0.4 ‰, n = 4) and +20.9 ‰ (±0.9 ‰, n = 5).

Clusters of three to five spots (within an area of <1 mm^2), were focused on enameloid, dentine and basal tissues of four holocephalan teeth (Fig. 4). Occasionally, one or more analytical spots missed the tissue targeted and average values were determined from remaining spot analyses. Average $\delta^{18}O$ values of spots (n = 5) targeting enameloid tissues in tooth MTM1-H1 produced values for spot clusters of +9.2 ±0.9 and +18.0 ±0.2 ‰ (Fig. 5A). The same enameloid tissue in sample MTM1-H9 was analysed, with individual clusters comprising two to three spots from four areas of the tooth (Fig. 5B) producing average $\delta^{18}O$ values between +21.4 ±0.7 and +21.8 ±0.1 ‰. Dentine was analysed in all four holocephalan teeth with an average $\delta^{18}O$ value of +17.9 ±1.4 ‰ (1σ, n = 35). No consistent differences in $\delta^{18}O$ are present between upper dentine, close to the occlusal surface of the tooth, and lower dentine tissues, located toward the basal body (Fig. 5). The enamel of three protacrodont teeth was tested using clusters of three to four spots and exhibited average $\delta^{18}O$ values of +17.9 ±0.4 ‰ (n = 3), +18.9 ±0.2 ‰ (n = 3) and +19.2 ±0.3 ‰ (n = 3) (Figs. 4, 6b). The dentine tissues in one tooth (1984-Dh1) showed a progressive depletion in ^{18}O from near the cusp apex (+16.2 ±0.2 ‰) to less mineralised dentine in the basal tissues (+13.8 ±0.5 ‰) (Fig. 4). A similar decrease in $\delta^{18}O$ is seen over 10 individual spots in an *Ageleodus* shark tooth (AG1, Fig. 6C), which presented a general trend in $\delta^{18}O$ from +17.3 ‰ in the cusp dentine, to +8.3 ‰ in the basal tissue. Three sets of analyses were performed on the dentine tissue of

three cladodont cusps, which showed average $\delta^{18}O$ values between +7.5 ±2.1 (n = 4) and +11.5 ±2.7 (n = 4) ‰ (Table 2).

Two sets of $\delta^{18}O$ values were recorded from different areas on a Famennian shark spine, a series of three spots near the margin of the spine (average +16.5 ±0.3 ‰, n = 4) and three spots located centrally (+18.5 ±0.4 ‰, n = 3). An average $\delta^{18}O$ value of +20.3 ‰ was recorded for scale crown surface tissues across different taxa from the Tournaisian samples. A difference of up to 2.1 ‰ was observed between spots on individual tissues. Dentine tissues from a Famennian protacrodont scale (+12.8 ±1.0 ‰, n = 2), Tournaisian lungfish (+8.8 ±1.9 ‰, n = 3 and +14.9 ±1.3 ‰, n = 5) and an acanthodian scale (+16.7 ±1.3 ‰) recorded $\delta^{18}O$ values consistently lower than the tissues close to the crown surfaces of the scales.

5. Discussion

5.1. Comparison of GIRMS and SIMS $\delta^{18}O$ analyses

Traditional GIRMS targets the PO_4^{3-} group and eliminates analysis of any less stable oxygen compounds (carbonate, organics, water) (Firsching, 1961; Wright and Hoering, 1989; Crowson et al., 1991; O'Neil et al., 1994). The use of whole vertebrate microfossils, in order to obtain minimum sample masses (~0.3-1 mg) required for this method, can be problematic. Potential differences in the O-isotopic signal of fossilised phosphate tissues may be masked when vertebrate bioapatite is homogenised. The highly permeable and porous nature of fossil dentine, which is the bulk component of fossil teeth and dermal denticles, is highly susceptible to physical and chemical alteration (Kohn and Cerling, 2002; Koch et al., 2007). This susceptibility results, in part, from significant porosity and permeability increasing potential isotopic exchange between bioapatite and circulating fluids associated with

399 diagenesis, as well as the potential for microbe mediated phosphate precipitation and
400 alteration (Kolodny et al., 1983; Kastner et al., 1990; Blake et al., 1997, 1998; Zazzo
401 et al., 2003).

402 The use of SIMS, as an alternative method for obtaining targeted $\delta^{18}O$ data
403 from fossil bioapatite, is advantageous where fossil yields are below the mass
404 required by GIRMS methods and when samples comprise different tissues (Wenzel
405 et al., 2000; Trotter et al., 2008; 2015). However, SIMS indiscriminately analyses
406 any oxygen-bearing compounds, including PO_4^{3-}, CO_3^{2-} and OH^- present within
407 bioapatite (Passey and Cerling, 2006; Aubert et al., 2012). The presence of the CO_3^{2-}
408 anion in bioapatite (either primary or as a secondary cement) can be particularly
409 problematic as it is more susceptible to diagenetic alteration than PO_4^{3-}, with the C-O
410 bond comparably weaker than the P-O bond (e.g. Iacumin et al., 1996).

411 Recent work by Wheeley et al. (2012) suggested $\delta^{18}O_{conodont}$ values obtained
412 from SIMS were comparable with those of GIRMS for Silurian conodonts. However,
413 it must be noted, offsets of ~1 ‰ between SIMS and GIRMS methods were
414 observed in some Silurian conodont genera (Wheeley et al., 2012). Subsequent work
415 by Trotter et al. (2015) showed an average offset of 0.6 ± 0.2 ‰ between the two
416 methodologies, similar to earlier work of 0.7 ‰ (Trotter et al., 2008). Published data
417 are currently considered insufficient to fully assess the presence and/or reasons for
418 any discrepancies; however, it appears small but measurable offsets exist. Here
419 fragments from a single crystal of Durango apatite were utilised to calibrate SIMS
420 analyses. GIRMS analysis gave an average $\delta^{18}O$ value of +9.9 ‰ (± 0.3 ‰, 1σ) from
421 triplicate analysis of three individual fragments of the same crystal, within error of
422 the published value of +9.8 ‰ reported by Rigo et al. (2012). GIRMS analysis of the
423 conodont genera *Ancyrodella* (+19.0 ±0.2 ‰) indicated a <0.2 ‰ difference when

compared to the $\delta^{18}O$ values obtained from SIMS of both *Ancyrodella* (+19.2 ‰±0.3 ‰) and *Palmatolepis* (+19.1 ‰) P_1 conodont elements from the same sample. The $\delta^{18}O_{conodont}$ values resolved from the two methods indicate valid comparisons can be made between SIMS and GIRMS analyses within error.

5.2. Canning Basin $\delta^{18}O_{conodont}$ values in a global context

The presence of open marine conditions in the Canning Basin, in the Late Devonian and Early Carboniferous, is important if $\delta^{18}O_{conodont}$ values are to be used as a globally representative baseline to assess the validity and palaeoenvironmental relevance of $\delta^{18}O$ values from vertebrate microfossils. The significant faunal cosmopolitanism found in ammonoid (Becker, 2000), conodont (Nicoll and Druce, 1979; Klapper, 2006) and vertebrate microfossil taxa (Turner, 1982; Trinajstic and George, 2009; Hairapetian et al., 2015; Roelofs et al., 2015, 2016; Trinajstic et al., 2015) in the Late Devonian and Early Carboniferous suggests that pathways existed for significant faunal exchange. Furthermore, the recovery, from the Lennard Shelf, of globally correlative carbon isotope signatures associated with the Kellwasser Event (Stephens and Sumner, 2003; Playton et al., 2013; George et al., 2014; Hillbun et al., 2015), and presence of a significant regression (Talent et al., 1993) and negative $\delta^{13}C$ excursion (Andrew et al., 1994) related to the Hangenberg Event, are all suggestive of a local marine system coupled to global oceanic conditions. Despite these indicators of an open marine system, the $\delta^{18}O_{conodont}$ values from Frasnian conodont Zone 11 (*jamieae* CZ) in the Canning Basin (+19.1-19.5 ‰) are approximately 1-1.5 ‰ higher than the $\delta^{18}O_{conodont}$ values (normalised to NBS 120c = +21.7 ‰) from latitudinally equivalent sites reported in Joachimski et al. (2004, 2009). The difference between the Canning Basin CZ 11 values and other sites may

be due to local variations in temperature and salinity and demonstrate the importance of natural global variations in water composition, particularly when constructing composite isotope curves. In contrast to the Frasnian sample, a paucity of conodont elements from the Famennian and Tournaisian makes it difficult for well constrained ages and, therefore, direct comparison of Canning Basin $\delta^{18}O_{conodont}$ with coeval global values. The Oscar Hill locality, from which the Famennian samples were taken, suggested deposition occurred during the latest Famennian based on conodont elements (*praesulcata* CZ, Nicoll and Druce, 1979). An average $\delta^{18}O_{conodont}$ value of +19.6 ‰ is comparable to values from other latitudinally similar sites from the *praesulcata* CZ from the Cantabrian Mountains, Spain (~+19.4 ‰) and Montagne Noire, France (~+17.6-19.5 ‰) (Buggisch et al., 2008; values were corrected by –0.7 ‰ to account for a difference in the reported $\delta^{18}O$ of standard NBS 120c). An early Tournaisian age for the Carboniferous sample was inferred from conodont and vertebrate microfossil remains. The average $\delta^{18}O$ value for *C. cavusformis* P_1-elements tested was +20.4 ±0.9 ‰. This is similar to the $\delta^{18}O_{conodonts}$ from the *sulcata* CZ interval (~+19.7-20.5 ‰, values were corrected by –0.7 ‰ to account for a difference in $\delta^{18}O$ of standard NBS 120c) in the Cantabrian Mountains, Spain (Buggisch et al., 2008). The results indicate that conodonts from the Frasnian to the Tournaisian in the Canning Basin are preserving isotopic signatures similar to conodonts from other pan tropical sites.

5.3. $\delta^{18}O$ variation in vertebrate microfossil tissues

The enameloid and dentine of four holocephalan teeth, all attributed to the same species, showed significant differences in $\delta^{18}O$ values as a result of histology, and therefore, mineral composition and susceptibility to diagenesis. The dense

enameloid tissue present in holocephalan teeth is similar in hardness to that of enamel (Ishiyama et al., 2012) and comprises the outer layer of the crown as well as pore linings penetrating the crown (Fig. 5). The $\delta^{18}O$ values obtained (via SIMS) adjacent to pore canals produced more consistent results (mean value of +21.5 ±0.2 ‰ for pore enameloid) than the outer mineralised layer of the crown, where $\delta^{18}O$ averages of spot clusters varied between +5.9 ±2.2 and +19.5 ±0.2 ‰. The enameloid tissue found along the outer surface of tooth MTM1-H1 (Fig. 5A) shows slight (spot no. 21-25) to considerably depletion (spot no. 1-5) of ^{18}O compared to co-occurring conodont $\delta^{18}O$ values. As this is not seen on the non-exposed side of the tooth MTM1-H9 from the same sample, it may represent alteration of the outer tissues prior to burial. There is also the potential for these values to be analytical artefacts due to topography induced through the differential polishing of the tooth and resin, or may result from diagenetic alteration, as the more discoloured areas in the tooth commonly show lower $\delta^{18}O$ values (Fig. 5B). Recent work has indicated that apparently well-preserved (i.e. lustrous) hypermineralised fossil tissues (e.g. Žigaitė et al., 2015) may not necessarily be indicative of pristine geochemistry. The presence of variable 'staining' in the teeth may reflect diagenetic mineralisation or alteration and may explain the significantly lower $\delta^{18}O$ values in peripheral hypermineralised tissues.

In general, the pore enameloid (Fig. 5B spot no. 4, 11-13, 17-18) of the holocephalan teeth analysed appears to more reliably preserve the original oxygen isotope ratios in comparison to the outer enameloid tissues (Fig. 5B spot no. 1-3, 5-7, 14-16), which are more readily exposed to post-mortem (or post-shedding), as well as burial, processes. The dentine tissue analysed from four holocephalan (Table 2) did not show any consistency in $\delta^{18}O$ values between individual teeth (Table 2). In

addition the most significant degree of $\delta^{18}O$ variation came from a single tooth (MTM1-H1). Here three areas within the tooth (MTM1-H1) were analysed. The first cluster of spots (Fig. 5a spot no. 6-10; +15.8 ±0.8 ‰) located in the cusp dentine; the second spot cluster (Fig. 5a spot no. 11-15; +19.5 ±0.2 ‰) present in an area of osteodentine; and a third spot cluster in the basal tissue (Fig. 5a spot no. 16-20; +17.6 ±0.1 ‰). Of these, the spot cluster at the basal area of HTM-H1 produced an average $\delta^{18}O$ value (+19.5 ±0.2 ‰ n = 5) comparable to average $\delta^{18}O_{conodont}$ from the same sample +20.3 ±0.8 ‰. The high $\delta^{18}O$ value may indicate that parts of the basal tissue, even though primarily consisting of permeable dentine, may be capable of preserving the original isotopic signatures under appropriate conditions.

The general structure of acrodin present in the tooth tip of many palaeonisciform fish is similar to the woven structure of enamel in elasmobranchs (Ripa et al., 1972; Ørvig, 1978a; Reif, 1985; Sasagawa et al., 2012) and thereby prospective in terms of resistance to diagenetic modification or disruption of isotopic signatures. The $\delta^{18}O$ values obtained from four spot analyses of the acrodin tip of a tooth (Mt-4 PN) support this histological robustness with a $\delta^{18}O$ value (+20.7 ±0.2 ‰ n = 4) and a standard deviation (1σ = ±0.5 ‰) comparable with associated conodonts (Fig. 6A, Table 2). The $\delta^{18}O$ value for the palaeoniscoid tooth dentine is depleted in ^{18}O (+15.9 ± 0.9 ‰) and similar to values from dentine in associated vertebrate microfossil taxa.

SIMS analyses were conducted on a range of scales belonging to acanthodians, chondrichthyan and palaeoniscoids. Scales attributed to each of these groups hosted $\delta^{18}O$ values within 1 ‰ of coeval conodont values (Fig. 4), which indicate that some scale tissues are preserving primary isotopic signatures. However, identifying the tissues that host these signatures is difficult as the spot size from the

SIMS beam is larger than some of the targeted tissues. This causes a degree of ambiguity in the $\delta^{18}O$ results due to the unquantifiable influence of surrounding tissues. The presence of ganoine, a tissue homologous with enamel (Qu et al., 2013), in some palaeoniscoid fish may explain the relatively high average $\delta^{18}O$ value of +19.5 ±1.3 ‰. Reconciling the average $\delta^{18}O$ value of +20.9 ±1.6 ‰ for the acanthodian scale (1984-04 Ac, Fig. 4) analysed is difficult, as scales of this taxa typically lack hypermineralised tissues and instead comprise an acellular bone base and a dentine layer covering the crown (Sire et al., 2009). Hypermineralised tissues such as ganoine have been reported in Palaeozoic acanthodians (e.g. Richter and Smith, 1995), which highlights the need for individual scales to be analysed rather than relying on the generalised histology of particular taxa. Overall, the results obtained from scales indicate that multiple taxa have the potential to be used to elicit apparently original isotopic data and interpret ancient environmental conditions.

5.4. Comparison of GIRMS and SIMS $\delta^{18}O$ analyses of vertebrate microfossils

As dentine tissues constitute the bulk of the vertebrate microfossils tested here, it is expected that results from GIRMS would be comparable to SIMS analyses of dentine from the same sample if the greater part of the signal detected by SIMS was from phosphate. This hypothesis is not fully supported by co-analysed fossils here (Fig. 7). Only two of the six analysed fossils produced average dentine $\delta^{18}O$ SIMS values within <1 ‰ of the GIRMS values. This is likely due to an insufficient number of spots, which were unable to encompass the full range of O-isotope variation within a single fossil. SIMS analysis of the lungfish scale (MT4-LPSi, Fig. 7) highlights the significant variation even within a small cluster of spots (±1.9 ‰ n = 3, ±1.3 ‰ n = 5). The potential for the alteration of PO_4 (since GIRMS analyses

549 are lower than coeval conodonts inhabiting the same water mass, see Section 5.5)
550 and contributions from other altered O-bearing compounds suggests SIMS and
551 GIRMS may not be comparable for heterogeneous tissues. Specific analysis of
552 hypermineralised tissues using both GIRMS and SIMS is required to determine if the
553 variation in hypermineralised tissue is low enough to produce comparable results
554 between the methods.
555
556 *5.5. Diagenetic influences*
557 Whole vertebrate microfossils analysed using GIRMS are commonly
558 depleted in ^{18}O when compared to coeval conodont elements (Žigaitė et al., 2010;
559 Barham et al., 2012a, b; Fischer et al., 2013). Since it has been demonstrated that
560 modern fish precipitate bioapatite in isotopic equilibrium with ambient water
561 (Kolodny et al., 1983; Vennemann et al., 2001; Puceat et al., 2010), and the
562 palaeoecology of many of the taxa are thought to overlap with those of coeval
563 conodonts, the lower $\delta^{18}O$ values are interpreted to have occurred as a consequence
564 of diagenetic changes in the less mineralised tissues. The 2.4 and 2.5 ‰ average
565 offsets found for Famennian and Tournaisian specimens examined herein (Fig. 3),
566 respectively, are close to those reported between Silurian conodonts and fish scales
567 (2.5 ‰; Žigaitė et al., 2010). The low colour alteration index (CAI) of the Silurian
568 conodonts (<1.5; Žigaitė et al., 2010) indicate thermally immature sediments, similar
569 to what is found in the Canning Basin, and may explain the similarity of the
570 discrepancy in $\delta^{18}O$ values. Moreover, Barham et al. (2012a) reported a more
571 significant depletion in ^{18}O from Mississippian, Viséan ichthyoliths from Ireland that
572 were associated with conodonts with CAI of >5, and indicated that the lower $\delta^{18}O$
573 values were influenced, but not necessarily controlled, by increasing diagenesis and

thermal alteration. It is difficult to extrapolate the results of thermal alteration from conodonts to vertebrate microfossils given the significant taxonomic differences between these groups. However, significant degrees of homology have been identified between the hypermineralised tissues of vertebrates and conodont hyaline tissue (Donoghue, 1998; Donoghue et al., 2000; Nemliher and Kallaste, 2012). Therefore, it is not unreasonable to expect the preserved phosphate in both conodont and vertebrate hard tissues would be affected in a similar fashion to thermal maturation processes. Given the similar magnitude of conodont-vertebrate microfossil $\delta^{18}O$ offset in thermally mature (CAI ~5.5 in Barham et al., 2012a reported $\delta^{18}O$ offset of 2.9 ‰) and immature regions (CAI <1.5; offset of 2.5 ‰ from Žigaitė et al., 2010; 2.4 and 2.5 ‰ offsets found herein), it can be assumed that there is no linear correlation between thermal maturation and depletion of $\delta^{18}O$ in vertebrate microfossil tissues.

The lower $\delta^{18}O$ values of vertebrate microfossils may be influenced by the susceptibility of their fossil tissues to chemical processes (Ayliffe et al., 1994; Wang and Cerling, 1994; Koch et al., 1997; Kohn et al., 1999; Sharp et al., 2000; Kohn and Cerling, 2002; France and Owsley, 2015). Given the composition and porosity/permeability of their dentine tissues, recrystallization of existing minerals (Kolodny and Luz, 1991; Kolodny et al., 1996) as well as precipitation of secondary O-bearing minerals (Martill, 1988; Blake et al., 1997; Kohn et al., 1999; Trueman and Palmer, 2003), both with theoretically different O-isotope compositions, are more significant considerations for vertebrate microfossils during early diagenesis (Koch et al., 1997; Sharp et al., 2000; Zazzo et al., 2004). The extent to which these aforementioned causes of alteration affect O-isotope ratios will be largely determined by original structure and composition of the analysed tissues (e.g. Kohn

and Cerling, 2002). Oxygen in apatite is present in the PO_4, CO_3 and OH groups (Driessens and Verbeeck, 1990). The phosphate component provides the most stable O-bond with no isotopic exchange observed in low temperature inorganic systems (Kolodny et al., 1983; Shemesh et al., 1988). The oxygen in carbonate however is susceptible to diagenetically induced fractionation (Luz et al., 1984; Nelson et al., 1986; Kolodny and Luz, 1991; Barrick and Showers, 1994, 1995; Wang and Cerling, 1994; Fricke et al. 1998; Kohn et al., 1999). Occurring at around 2-6 wt % in bone and dentine (LeGeros and LeGeros, 1984; Driessens and Verbeeck, 1990), diagenetic affects may influence the final $\delta^{18}O$ values measured by SIMS. The effects of OH^- fractionation and substitution by other compounds such as CO^3 (Kohn et al., 1999) however, will not likely cause significant variation in the final $\delta^{18}O$ values as the wt % in dentine and bone is low (<1.6 wt %, Cerling and Sharp, 1996).

SIMS $\delta^{18}O$ analysis of modern shark teeth (Žigaitė and Whitehouse, 2014) identified average $\delta^{18}O$ variation of 1.2 ‰ within the dentine tissue. Mean variation between the parallel bundled enameloid (+21.2-23.1 ‰) and dentine tissue (+20.6-21.8 ‰) was also recorded. Žigaitė and Whitehouse (2014) noted the use of H_2O_2 in the pre-treatment cleaning process may have contributed to variation in the $\delta^{18}O$ values. However, it was concluded that organic matter, which is typically ^{18}O depleted, was the likely cause of this variation. The fossil shark and holocephali teeth tested here also showed significant discrepancies between tissues, as well as depletion in ^{18}O (Figs. 4, 5b, 6). However, such variation in the fossil specimens analysed here, cannot be attributed to original organic material as this would have degraded to the point where it would be undetectable, although decay products could have influenced the isotope ratios. Interestingly, analysis of teeth taken from freshly caught sharks (Vennemann et al., 2001) recorded comparable values between the

624 dentine and enamel tissues using GIRMS. The isolation of PO_4 eliminates the
625 influence of ^{18}O depleted organic matter, which may have resulted in $\delta^{18}O$ variation
626 between the dentine and enamel. Work by Zazzo et al. (2003), has demonstrated
627 fractionation of phosphate within bone can occur within a few days post-mortem
628 under oxic conditions, with the presence of microbial enzyme activity significantly
629 increasing the rate of oxygen isotope exchange. In contrast, enamel was found to be
630 significantly resistant to changes in the original oxygen isotope ratios (Zazzo et al.,
631 2003). The susceptibility for isotopic alteration under microbially-mediated
632 conditions for tissues with originally higher organic matter content, could explain the
633 lower oxygen isotope values of the dentine of the shed teeth analysed by Žigaitė and
634 Whitehouse (2014). Microbial "catalysts" have been previously used to explain the
635 alteration of PO_4 $\delta^{18}O$ in bioapatite (Kolodny et al., 1983; Kastner et al., 1990). The
636 Upper Devonian and Lower Carboniferous vertebrate microfossil elements analysed
637 here were obtained from limestones formed in well oxygenated shallow water
638 marine settings (Druce and Radke, 1979). Given the lack of thermal maturity or any
639 evidence for fluid alteration of the sequences studied, microbially-induced alteration
640 within incompletely mineralised tissues in vertebrate microfossils ex-vivo and/or
641 during early diagenesis (eogenesis) must be considered a plausible mechanism for
642 lower $\delta^{18}O$-values.

643 Evidence for recent weathering processes affecting $\delta^{18}O$-values is present in
644 one of the holocephalan teeth (MTM1-H9, Fig. 5B), which had a portion of the
645 occluso-labial face of the crown protruding from a rock. It is difficult to constrain the
646 length of time the tooth was exposed, however it is likely that it was affected by a
647 range of weathering processes including frequent scrub fires and interaction with
648 meteoric fluids. The effect of exposure was evident with the outer enameloid layer of

649 the tooth producing values progressively depleted in ^{18}O toward the exposed surface.
650 The low $\delta^{18}O$ values between +5.2-5.9 ‰ (Fig. 5B spot no. 1-3) at the exposed face
651 correspond to significant degradation of the enameloid and dentine. However, the
652 affected area was small and the dentine within the tooth (+19.5 ±0.7 ‰) was found
653 to be comparable to the outer enameloid surface on the non-exposed face (+21.4 ‰,
654 Fig. 6b). This suggests relative localisation of alteration and overall robustness of the
655 tissue to short-term abiotic processes.
656
657 *5.6. Palaeoecological influences*
658 Understanding the biology of ancient sharks and fish as well as the
659 environments they inhabited is important to contextualise variation present in tissues,
660 particularly hypermineralised tissues, where primary isotope values are thought to be
661 original. Glaciation, resulting in the preferential locking of ^{16}O in terrestrial ice-
662 sheets, was present during the late Famennian and early Tournaisian (Kaiser et al.,
663 2006). Evidence suggests these glacial conditions were not as extensive as the
664 modern climate state (Isaacson et al., 2008), hence a $\delta^{18}O_{seawater}$ offset of –0.5 ‰
665 (VSMOW) is inferred to account for greater ^{16}O concentrations in the oceans than in
666 the present-day. Assuming these glacial conditions and subsequent offset to
667 $\delta^{18}O_{seawater}$, average $\delta^{18}O$ values (+17.8, +18.9 and +19.2 ‰) from protacrodont tooth
668 enamel (uncorrected for diagenetic alteration due to their hypermineralised
669 condition) indicate palaeotemperatures of between 34 and 42° C (calculated using
670 the equation of Lécuyer et al., 2013). Such sea-surface temperatures are considerably
671 higher than those calculated from coeval conodont (25 and 29° C using the equation
672 of Lécuyer et al., 2013).

673 Enrichment of ^{16}O as a result of bioapatite precipitation from a water mass
674 influenced by meteoric fluids in both the Protacrodont (Fig. 5b) teeth cannot be
675 easily dismissed. However, this would imply migratory habits for the taxa, as the
676 fauna and facies of the Laurel Formation indicate an exclusively marine setting
677 (Druce and Radke, 1979). Similar to the habits of extant shark species such as
678 *Carcharhinus leucas* (bull shark) (Copeia, 1971) and *Glyphis gangeticus (*Ganges
679 shark) (Compagno, 1997), Palaeozoic shark taxa are known to have inhabited
680 freshwater environments on both a permanent (e.g. Xenacanths, Ginter et al., 2010;
681 members of the *Ageleodus* genus, Downs and Daeschler, 2001) and temporary basis
682 (e.g. *Lissodus*, Fischer et al., 2013). Strontium isotope analysis has been previously
683 employed on chondrichthyan taxa (Scharer et al., 2012; Fischer et al., 2013; 2014;
684 Raoult et al., 2016) in order to quantify the salinity variable. It may be necessary to
685 include this form of analysis in order to isolate the palaeotemperature signal of
686 vertebrate microfossil O-isotope data when incorporating fossil taxa known to
687 inhabit different environments.

688 Significant ecological differences within fully marine extant shark genera are
689 reflected in the O-isotope ratios of the mineralised tissues (Vennemann et al., 2001).
690 The potential migration of ancient sharks across latitudes or water depths must also
691 be taken into account when interpreting O-isotope data from nektonic fossil taxa.
692 Significant migratory behaviour is observed in extant taxa such as *Odontaspis ferox*
693 (Fergusson et al., 2008), which has been found at depths of 850 m as well as very
694 shallow coastal waters. In addition, members of the species *Carcharodon carcharias*
695 (great white shark) have been frequently observed migrating long distances, in some
696 cases over 20,000 km in less than a year (Bonfil et al., 2005). Migratory issues of
697 extinct species may be compounded in groups such as the Ctenicanthiforms where

698 tooth development is slower than that observed in modern sharks (Williams, 2001;
699 Botella et al., 2009). Analysis of species with fast tooth replacement rates may
700 mitigate some migratory factors as teeth are more likely to preserve local conditions.
701 Tooth formation can be as quick as 9-12 days within some extant selachians (Moss,
702 1967); however, determining similar tooth replacement in Palaeozoic species is
703 currently difficult to ascertain.
704
705 **6. Conclusions**
706 The hypermineralised bioapatite present in vertebrate teeth and scales
707 provides a proxy capable of reconstructing marine oxygen isotope records from the
708 middle Palaeozoic to the modern day. The densely crystalline tissues that form
709 enamel, enameloid and acrodin show the greatest potential of preserving original
710 oxygen isotope signatures. Results presented herein from a broad range of taxa
711 (scales of acanthodians as well as the scales and teeth of chondrichthyans and
712 actinopterygians) indicate eliciting palaeoenvironmental data from other vertebrate
713 groups is likely.
714 The utilisation of SIMS, which permits tissue specific analysis, suggests
715 dentine tissue is more susceptible to alteration due to a higher porosity and
716 permeability inherited from an originally high organic component. The low CAI of
717 conodont fossils analysed here suggests thermal maturation is not the dominant
718 factor in the lower $\delta^{18}O$ values obtained from vertebrate microfossils. Instead, this
719 work suggests ex-vivo microbial activity may be a more likely factor in the alteration
720 of the original oxygen isotope ratios.
721 Going forward, it is clear that a range of Palaeozoic vertebrate groups offer
722 an alternative tool for reconstructing palaeoenvironmental conditions (watermass

palaeotemperature and palaeohydrological condition). In addition, the presence of potentially original isotopic signatures provides a basis for applications in chemostratigraphy where conodonts are rare or absent. SIMS analysis of targeted hypermineralised vertebrate microfossil tissues can resolve original O-isotope values, and therefore can be used in a similar fashion to, and correlated with, $\delta^{18}O_{conodont}$. However, minimising potential $\delta^{18}O$ variation as a consequence of species dependant factors such as migratory habits remains critical. Ideally analyses should include multiple species and comparisons to co-occurring or coeval conodonts from other areas.

Acknowledgments

Thanks to Daniele Lutz from the GeoZentrum Nordbayern, University of Erlangen-Nürnberg, Germany for aiding in the preparation of the fossil material for analysis. BR would like to thank the anonymous reviewers of his dissertation for their helpful comments. In addition, a thank you to the editor Thomas Algeo and the anonymous reviewers for their invaluable comments regarding the manuscript. The authors acknowledge the use of equipment, scientific and technical assistance of the Curtin University Electron Microscope Facility, which has been partially funded by the University, State and Commonwealth Governments. In addition the authors would also like to acknowledge the facilities, and the scientific and technical assistance of the Australian Microscopy & Microanalysis Research Facility at the Centre for Microscopy, Characterisation & Analysis, The University of Western Australia, a facility funded by the University, State and Commonwealth Governments. The authors are also indebted to Catherine Boisvert, Alison Edmunds and the Melbourne Aquarium for providing access to water samples and naturally shed shark teeth,

collected during routine cleaning. Further appreciation goes to Bradley McDonald for access to Durango apatite. The authors also acknowledge support from MRIWA, WA ERA, CSIRO, Chevron Australia Business Unit, Chevron Energy Technology Company, National Science Foundation and the Geological Survey of Western Australia. We would also like to thank the owners of Brooking Springs and Laurel Downs stations for allowing access to outcrops. BR recognises the receipt of an Australian Postgraduate Award as well as a Curtin Completion Scholarship. This research was funded under Australian Research Council grant DP 110101127.

References

Andrew, A., Hamilton, P., Mawson, R., Talent, J., Whitford, D., 1994. Isotopic correlation tools in the mid-Palaeozoic and their relation to extinction events. Australian Petroleum Exploration Association Journal 34, 268–268.

Aubert M., Williams I.S., Boljkovac K., Moffat I., 2012 In situ oxygen isotope micro-analysis of faunal material and human teeth using a SHRIMP II: a new tool for palaeo-ecology and archaeology. Journal of Archaeological Science 39, 3184–3194.

Ayliffe, L.K., Chivas, A., Leakey, M.G., 1994. The retention of primary oxygen isotope compositions of fossil elephant skeletal phopshate. Geochimica et Cosmochimica Acta 58, 5291–5298.

Auclair, A., Joachimski, M.M., Lécuyer, C., 2003. Deciphering kinetic, metabolic and environmental controls on stable isotope fractionations between seawater and the shell of *Terebratalia transversa* (Brachiopoda), Chemical Geology 202, 59–78.

772 Azmy, K., Veizer, J., Bassett, M.G., Copper, P., 1998. Oxygen and carbon isotopic
773 composition of Silurian brachiopods: implications for coeval seawater and
774 glaciations. Geological Society of America Bulletin 110, 1499–1512.
775 Barham, M., Joachimski, M., Murray, J., Williams, D., 2012a. Diagenetic alteration
776 of the structure and δ 18 O signature of Palaeozoic fish and conodont apatite:
777 Potential use for corrected isotope signatures in palaeoenvironmental
778 interpretation. Chemical Geology 298, 11–19.
779 Barham, M., Murray, J., Joachimski, M., Williams, D., 2012b. The onset of the
780 Permo-Carboniferous glaciation: reconciling global stratigraphic evidence
781 with biogenic apatite $\delta^{18}O$ records in the late Visean. Journal of the
782 Geological Society 169, 119–122.
783 Barrick, R.E., Showers, W.J., 1994. Thermophysiology of Tyrannosaurus rex:
784 evidence from oxygen isotopes. Science 265, 222–224.
785 Barrick, R.E., Showers, W.J., 1995. Oxygen isotope variability in juvenile dinosaurs
786 (Hypacrosaurus): evidence for thermoregulation. Paleobiology 21, 552–560.
787 Becker, R., House, M., 2009. Devonian ammonoid biostratigraphy of the Canning
788 Basin. Geological Survey of Western Australia, Bulletin 145, 415–439.
789 Billon-Bruyat, J.P., Lécuyer, C., Martineau, F., Mazin,, J.M., 2005. Oxygen isotope
790 compositions of Late Jurassic vertebrate remains from lithographic
791 limestones of western Europe: implications for the ecology of fish, turtles,
792 and crocodilians. Palaeogeography, Palaeoclimatology, Palaeoecology 216,
793 359–375.
794 Blake, R.E., O'neil, J.R., Garcia, G.A., 1997. Oxygen isotope systematics of
795 biologically mediated reactions of phosphate: I. Microbial degradation of

organophosphorus compounds. Geochimica et Cosmochimica Acta, 61, 4411–4422.

Blake, R.E., O'Neil, J.R., Garcia, G.A. 1998. Effects of microbial activity on the $\delta^{18}O$ of dissolved inorganic phosphate and textural features of synthetic apatites. American Mineralogist, 83, 1516–1531.

Bonfil, R., Meÿer, M., Scholl, M.C., Johnson, R., O'Brien, S., Oosthuizen, H., Swanson, S., Kotze, D., Paterson, M., 2005. Transoceanic migration, spatial dynamics, and population linkages of white sharks. Science 310,100–103.

Brady, A., 2011. Laser Ablation as a Valuable Tool in the Stable Isotope Analysis of Archaeological Material. Totem: The University of Western Ontario Journal of Anthropology 12, 27–32.

Brand, U., 1989. Biogeochemistry of Late Paleozoic North American brachiopods and secular variation of seawater composition. Biogeochemistry 7, 159–193.

Brand, U., 2004. Carbon, oxygen and strontium isotopes in Paleozoic carbonate components: an evaluation of original seawater-chemistry proxies. Chemical Geology 204, 23–44.

Brazeau, M.D., 2009. The braincase and jaws of a Devonian 'acanthodian' and modern gnathostome origins. Nature 457, 305–308

Brazeau, M.D, de Winter, V., 2015. The hyoid arch and braincase anatomy of Acanthodes support chondrichthyan affinity of 'acanthodians'. Proceedings of the Royal Society B: Biological Sciences 282, 2015–2210.

Buggisch, W., Joachimski, M.M., Sevastopulo, G., Morrow, J.R., 2008. Mississippian $\delta^{13}C$ carb and conodont apatite $\delta^{18}O$ records—their relation to the Late Palaeozoic Glaciation. Palaeogeography, Palaeoclimatology, Palaeoecology 268, 273–292.

821 Caplan, M.L., Bustin, R.M., 1999. Devonian - Carboniferous Hangenberg mass
822 extinction event, widespread organic-rich mudrock and anoxia: causes and
823 consequences. Palaeogeography, Palaeoclimatology, Palaeoecology 148,
824 187–207.
825 Caputo, M.V., Crowell, J.C., 1985. Migration of glacial centers across Gondwana
826 during Paleozoic Era. Geological Society of America Bulletin 96, 1020–
827 1036.
828 Carpenter, S.J., Lohmann, K.C., Holden, P., Walter, L.M., Huston, T.J., Halliday,
829 A.N., 1991. $\delta^{18}O$ values, $^{87}Sr^{86}Sr$ and Sr/Mg ratios of Late Devonian abiotic
830 marine calcite: Implications for the composition of ancient seawater.
831 Geochimica et Cosmochimica Acta 55, 1991–2010.
832 Cerling, T. E., Sharp, Z.D., 1996. Stable carbon and oxygen isotope analysis of fossil
833 tooth enamel using laser ablation. Palaeogeography, Palaeoclimatology,
834 Palaeoecology 126, 173-186.
835 Chen, B., Joachimski, M.M., Wang, X.D. Shen, S., Qi, Y., Qie, W., 2016. Ice
836 volume and paleoclimate history of the Late Paleozoic ice age from conodont
837 apatite oxygen isotopes from Naqing (Guizhou, China). Palaeogeography,
838 Palaeoecology, Palaeoclimatology 448, 151–161.
839 Compagno, L.J. 1997. Threatened fishes of the world: *Glyphis gangeticus* (Müller &
840 Henle, 1839) (Carcharhinidae). Environmental biology of fishes 49, 400–400.
841 Crowson, R.A., Showers W.J., Wright, E.K., Hoering, T.C., 1991. Preparation of
842 phosphate samples for oxygen isotope analysis. Analytical Chemistry 63,
843 2397–2400.

844 Cummins, R.C., Finnegan, S., Fike, D.A., Eiler, J.M., Fischer, W.W., 2014.
845 Carbonate clumped isotope constraints on Silurian ocean temperature and
846 seawater $\delta^{18}O$. Geochimica et Cosmochimica Acta 140, 241–258.
847 Davis, S.P., Finarelli, J.A., Coates, M.I., 2012, *Acanthodes* and shark-like conditions
848 in the last common ancestor of modern gnathostomes. Nature 486, 247–250.
849 Donoghue, P.C.J., 1998. Growth and patterning in the conodont skeleton.
850 Philosophical Transactions of the Royal Society of London 353, 633–666.
851 Donoghue, P.C.J., Forey, P.L., Aldridge, R.J., 2000. Conodont affinity and chordate
852 phylogeny. Biological Reviews 75, 191–251.
853 Downs, J.P., Daeschler, E.B., 2001. Variation within a large sample of *Ageleodus*
854 *pectinatus* teeth (Chondrichthyes) from the Late Devonian of Pennsylvania,
855 USA. Journal of Vertebrate Paleontology 21, 811–814.
856 Driessens F.C.M., Verbeek R.M.H., 1990. Biominerals. CRC Press, Boca Raton,
857 Florida, USA.
858 Dzik, J., 1991. Evolution of the oral apparatuses in the conodont chordates. Acta
859 Palaeontologica Polonica 36, 265–323.
860 Firsching, F.H., 1961. Precipitation of silver phosphate from homogeneous solution.
861 Analytical Chemistry 33, 873–874.
862 Fischer, J., Schneider, J.W., Hodnett, J.P.M., Elliott, D.K., Johnson, G.D., Voigt, S.,
863 Götze, J., 2014. Stable and radiogenic isotope analyses on shark teeth from
864 the Early to the Middle Permian (Sakmarian–Roadian) of the southwestern
865 USA. Historical Biology 26, 710–727.
866 Fischer, J., Schneider, J.W., Voigt, S., Joachimski, M.M., Tichomirowa, M., Tütken,
867 T., Götze, J., Berner, U., 2013. Oxygen and strontium isotopes from fossil

868 shark teeth: Environmental and ecological implications for Late Palaeozoic
869 European basins. Chemical Geology 342, 44–62.
870 Fischer, J., Voight, S., Franz, M., Schneider, J.W., Joachimski, M.M., Tichomirowa,
871 M., Götze, J., Furrer, H., 2012. Palaeoenvironments of the late Triassic
872 Rhaetian Sea: implications from oxygen and strontium isotopes of hybodont
873 shark teeth. Palaeogeography Palaeoclimatology Palaeoecology 353, 60–72.
874 France, C.A.M., Owsley, D.W., 2015. Stable carbon and oxygen isotope spacing
875 between bone and tooth collagen and hydroxyapatite in human archaeological
876 remains. International Journal of Osteoarchaeology 25, 299–312.
877 Fricke, H.C., Clyde, W.C., O'Neil, J.R., Gingerich, P.D., 1998. Evidence for rapid
878 climate change in North America during the latest Paleocene thermal
879 maximum: oxygen isotope compositions of biogenic phosphate from the
880 Bighorn Basin (Wyoming). Earth and Planetary Science Letters 160, 193–
881 208.
882 Gabbott, S. E., Aledridge, R.J., Theron, J.N., 1995. A giant conodont with preserved
883 muscle tissue from the Upper Ordovician of South Africa. Nature 374, 800–
884 803.
885 George, A.D., Chow, N., Trinajstic, K.M., 2014. Oxic facies and the Late Devonian
886 mass extinction, Canning Basin, Australia. Geology 42, 327–330.
887 Ginter, M., Hampe, O., Duffin, C.J., 2010. Paleozoic Elasmobranchii: Teeth. Pfeil.
888 Goldberg, M., Kulkarni, A.B., Young, M., Boskey, A., 2011. Dentin: Structure,
889 Composition and Mineralization: The role of dentin ECM in dentin formation
890 and mineralization. Frontiers in bioscience (Elite edition) 3, 711–735.
891 Goudemand, N., Orchard, M.J., Urdy, S., Bucher, H., Tafforeau, P., 2011.
892 Synchrotron-aided reconstruction of the conodont feeding apparatus and

893 implications for the mouth of the first vertebrates. Proceedings of the
894 National Academy of Sciences 108, 8720–8724.
895 Grimes, S.T., Mattey, D.P., Hooker, J.J., Collinson, M.E., 2003. Paleogene
896 paleoclimate reconstruction using oxygen isotopes from land and freshwater
897 organisms: the use of multiple paleoproxies. Geochimica et Cosmochimica
898 Acta, 67, 4033-4047.
899 Gruszczyński, M., Hałas, S., Hoffman, A., Małkowski, K., 1989. A brachiopod
900 calcite record of the oceanic carbon and oxygen isotope shifts at the
901 Permian/Triassic transition. Nature 337, 64–68.
902 Hairapetian, V., Roelofs, B.P., Trinajstic, K.M., Turner, S., 2015. Famennian
903 survivor turiniid thelodonts of North and East Gondwana. Geological
904 Society, London, Special Publications 423.
905 Hamlett, W.C., 1999. Sharks, skates, and rays: the biology of elasmobranch fishes.
906 JHU Press.
907 Hand, A.R., Frank, M.E., 2014. Fundamentals of Oral Histology and Physiology.
908 John Wiley & Sons.
909 Hays, P.D., Grossman, E.L., 1991. Oxygen isotopes in meteoric calcite cements as
910 indicators of continental paleoclimate. Geology 19, 441–444.
911 Hillbun, K., Playton, T.E., Tohver, E., Ratcliffe, K., Trinajstic, K., Roelofs, B.,
912 Caulfield-Kerney, S., Wray, D., Haines, P., Hocking, R., 2015. Upper
913 Kellwasser carbon isotope excursion pre-dates the F-F boundary in the Upper
914 Devonian Lennard Shelf carbonate system, Canning Basin, Western
915 Australia. Palaeogeography, Palaeoclimatology, Palaeoecology 438, 180–
916 190.

Iacumin, P., Bocherens, H., Mariotti, A., Longinelli, A., 1996. Oxygen isotope analyses of co-existing carbonate and phosphate in biogenic apatite: a way to monitor diagenetic alteration of bone phosphate? Earth and Planetary Science Letters 142, 1–6.

James, N.P., Bone, Y., Kyser, T.K., 1997. Brachiopod $\delta^{18}O$ values do reflect ambient oceanography: Lacepede Shelf, southern Australia. Geology 25, 551–554.

Janvier, P. 1996. Early vertebrates. Clarendon Press Oxford.

Jeppsson, L., Anehus, R., Fredholm, D., 1999. The optimal acetate buffered acetic acid technique for extracting phosphatic fossils. Journal of Paleontology, 964–972.

Joachimski, M., Breisig, S., Buggisch, W., Talent, J., Mawson, R., Gereke, M., Morrow, J., Day, J., Weddige, K., 2009. Devonian climate and reef evolution: insights from oxygen isotopes in apatite. Earth and Planetary Science Letters 284, 599–609.

Joachimski, M.M., Buggisch, W., 2002. Conodont apatite $\delta^{18}O$ signatures indicate climatic cooling as a trigger of the Late Devonian mass extinction. Geology 30, 711–714.

Joachimski, M. M., Lai, X., Shen, S., Jiang, H., Luo, G., Chen, B., Sun, Y., 2012. Climate warming in the latest Permian and the Permian–Triassic mass extinction. Geology 40, 195–198.

Joachimski, M.M., Lambert, L.L., 2015. Salinity contrast in the US midcontinent sea during Pennsylvanian glacio-eustatic highstands: Evidence from conodont apatite $\delta^{18}O$. Palaeogeography, Palaeoclimatology, Palaeoecology 433, 71–80.

941 Joachimski, M.M., Van Geldern, R., Breisig, S., Buggisch, W., Day, J., 2004.
942 Oxygen isotope evolution of biogenic calcite and apatite during the Middle
943 and Late Devonian. International Journal of Earth Sciences 93, 542–553.
944 Jones, D., Evans, A.R., Siu, K.K., Rayfield, E.J., Donoghue, P.C., 2012. The
945 sharpest tools in the box? Quantitative analysis of conodont element
946 functional morphology. Proceedings of the Royal Society of London B:
947 Biological Sciences 279, 2849–2854.
948 Kaiser, S.I., Steuber, T., Becker, R.T., 2008. Environmental change during the Late
949 Famennian and Early Tournaisian (Late Devonian - Early Carboniferous):
950 implications from stable isotopes and conodont biofacies in southern Europe.
951 Geological Journal 43, 241–260.
952 Kaiser, S.I., Steuber, T., Becker, R.T., Joachimski, M.M., 2006. Geochemical
953 evidence for major environmental change at the Devonian - Carboniferous
954 boundary in the Carnic Alps and the Rhenish Massif. Palaeogeography,
955 Palaeoclimatology, Palaeoecology 240, 146–160.
956 Karatajute-Talimaa, V., 1998. Determination methods for the exoskeletal remains of
957 early vertebrates. Fossil Record 1, 21–51.
958 Kastner, M., Garrison, R.E., Kolodny, Y., Reimers, C.E., Shemesh, A., 1990.
959 Coupled changes of oxygen isotopes in PO_4^{3-} and CO_3^{2-} in apatite, with
960 emphasis on the Monterey Formation, California. Phosphate deposits of the
961 world 3, 312–324.
962 Kita, N.T., Ushikubo, T., Fu, B., Valley, J.W., 2009. High precision SIMS oxygen
963 isotope analysis and the effect of sample topography. Chemical Geology 264,
964 43–57.

965 Klapper, G., 1988. The Montagne Noire Frasnian (Upper Devonian) conodont
966 succession. Journal of Paleontology 81, 513–537.
967 Klapper, G., 2007. Frasnian (Upper Devonian) conodont succession at Horse Spring
968 and correlative sections, Canning Basin, Western Australia. Journal of
969 Palaeontology 81, 513–527.
970 Koch, P.L., 2007. Isotopic study of the biology of modern and fossil
971 vertebrates. Stable isotopes in ecology and environmental science 2, 99–154.
972 Koch, P.L., Tuross, N., Fogel, M.L., 1997. The effects of sample treatment and
973 diagenesis on the isotopic integrity of carbonate in biogenic
974 hydroxylapatite. Journal of Archaeological Science 24, 417-429.
975 Kohn, M.J., Schoeninger, M.J., Barker, W.W., 1999. Altered states: effects of
976 diagenesis on fossil tooth chemistry. Geochimica et Cosmochimica Acta 63,
977 2737–2747.
978 Kohn, M.J., Cerling, T.E., 2002. Stable isotope compositions of biological
979 apatite. Reviews in mineralogy and geochemistry 48, 455–488.
980 Kolodny, Y., Luz, B., 1991. Oxygen isotopes in phosphates of fossil fish —
981 Devonian to Recent. In: Taylor, H.P., O'Neil, J.R., Kaplan, I.R. (Editors),
982 Stable Isotope Geochemistry: A Tribute to Samuel Epstein: The Geochemical
983 Society Special Publication 3, 105–119.
984 Kolodny, Y., Luz, B., Sander, M., Clemens, W.A. 1996. Dinosaur bones: fossils or
985 pseudomorphs? The pitfalls of physiology reconstruction from apatitic
986 fossils. Palaeogeography, Palaeoclimatology, Palaeoecology 126, 161-171.
987 Kolodny, Y., Luz, B., Navon, O., 1983. Oxygen isotope variations in phosphate of
988 biogenic apatites, I. Fish bone apatite—rechecking the rules of the game.
989 Earth and Planetary Science Letters 64, 398–404.

990 Kolodny, Y., Raab, M., 1988. Oxygen isotopes in phosphatic fish remains from
991 Israel: paleothermometry of tropical Cretaceous and Tertiary shelf
992 waters. Palaeogeography, Palaeoclimatology, Palaeoecology 64, 59-67.
993 Korte, C., Jones, P.J., Brand, U., Mertmann, D., Veizer, J., 2008. Oxygen isotope
994 values from high-latitudes: clues for Permian sea-surface temperature
995 gradients and Late Palaeozoic deglaciation. Palaeogeography,
996 Palaeoclimatology, Palaeoecology 269, 1–16.
997 LaPorte, D., Holmden, C., Patterson, W., Prokopiuk, T., Eglington, B., 2009.
998 Oxygen isotope analysis of phosphate: improved precision using TC/EA
999 CF-IRMS. Journal of mass spectrometry 44, 879–890.
1000 Lécuyer, C., Allemand, P., 1999. Modelling of the oxygen isotope evolution of
1001 seawater: implications for the climate interpretation of the $\delta^{18}O$ of marine
1002 sediments. Geochimica et Cosmochimica Acta 63, 351–361.
1003 Lécuyer, C., Amiot, R., Touzeau, A., Trotter, J., 2013. Calibration of the phosphate
1004 $\delta^{18}O$ thermometer with carbonate - water oxygen isotope fractionation
1005 equations. Chemical Geology 347, 217–226.
1006 Lecuyer, C., Fourel, F., Martineau, F., Amiot, R., Bernard, A., Daux, V., Escarguel,
1007 G., Morrison, J., 2007. High-precision determination of $^{18}O/^{16}O$ ratios of
1008 silver phosphate by EA-pyrolysis-IRMS continuous flow technique. Journal
1009 of Mass Spectrometry 42, 36–41.
1010 Lécuyer, C., Grandjean, P., O'Neil, J.R., Cappetta, H., Martineau, F., 1993. Thermal
1011 excursions in the ocean at the Cretaceous—Tertiary boundary (northern
1012 Morocco): $\delta^{18}O$ record of phosphatic fish debris. Palaeogeography,
1013 Palaeoclimatology, Palaeoecology 105, 235–243.

1014 Lécuyer, C., Picard, S., Garcia, J.-P., Sheppard, S.M.F., Grandjean, P., Dromart, G.,
1015 2003. Thermal evolution of Tethyan surface waters during the Middle-Late
1016 Jurassic: evidence from d18O values of marine fish teeth. Paleoceanography
1017 18, 1076–1091.
1018 LeGeros, R.Z., LeGeros, J.P., 1984. Phosphate minerals in human tissue. In: Nriagu
1019 J.O., Moore, P.B. (Editors). Phosphate Minerals. Springer-Verlag, New York,
1020 351–395.
1021 Lindström, M., 1964. Conodonts. *Elsevier Publishing Company*, Amsterdam.
1022 Lindström, M., Racheboeuf, P., Henry, J., 1974. Ordovician conodonts from the
1023 Postolonnec Formation (Crozon Peninsula, Massif Armoricain) and their
1024 stratigraphic significance. Geologica et Palaeontologica 8, 15–28.
1025 Luz, B., Kolodny, Y., Kovach, J., 1984. Oxygen isotope variations in phosphate of
1026 biogenic apatites, III. Conodonts. Earth and Planetary Science Letters 69,
1027 255–262.
1028 Martill, D.M., 1988. Preservation of fish in the Cretaceous Santana Formation of
1029 Brazil. Palaeontology 31, 1–18.
1030 Mii, H., Grossman, E.L., Yancey, T.E., 1997. Stable carbon and oxygen isotope
1031 shifts in Permian seas of West Spitsbergen-Global change or diagenetic
1032 artifact? Geology 25, 227–230.
1033 Mii, H., Grossman, E.L., Yancey, T.E., 1999. Carboniferous isotope stratigraphies of
1034 North America: Implications for Carboniferous paleoceanography and
1035 Mississippian glaciation. Geological Society of America Bulletin 111, 960–
1036 973.
1037 Nelson, B.K., DeNiro, M.J., Schoeninger, M.J., De Paolo, D.J., Hare, P.E., 1986.
1038 Effects of diagenesis on strontium, carbon, nitrogen and oxygen

concentration and isotopic composition of bone. Geochimica et Cosmochimica Acta 50, 1941–1949.

Nicoll, R.S., Druce, E.C., 1979. Conodonts from the Fairfield Group, Canning Basin, Western Australia. Australian Government Publishing Service.

Nemliher, J., Kallaste, T., 2012. Conodont bioapatite resembles vertebrate enamel by XRD properties. Estonian Journal of Earth Sciences 61, 191–192.

Nöth, S., 1998. Conodont color (CAI) versus microcrystalline and textural changes in Upper Triassic conodonts from Northwest Germany. Facies 38, 165–173.

O'Neil, J.R., Roe, L.J., Reinhard, E., Blake, R., 1994. A rapid and precise method of oxygen isotope analysis of biogenic phosphate. Israel Journal of Earth Sciences 43, 203–212.

Ørvig, T., 1978a. Microstructure and growth of the dermal skeleton in fossil actinopterygian fishes: *Boreosomus*, *Plegmolepis* and *Gyrolepis*. Zoologica Scripta 7, 125–144.

Ørvig, T., 1978b. Microstructure and Growth of the Dermal Skeleton in Fossil Actinopterygian Fishes: *Nephrotus* and *Colobodus*, with Remarks on the Dentition in Other Forms1. Zoologica scripta 7, 297–326.

Ørvig, T., 1980. Histologic studies of ostracoderms, placoderms and fossil elasmobranchs. Zoologica Scripta 9, 219–239.

Passey B. H., Cerling T. E., Schuster G., Robinson T. F., 2005. Inverse methods for estimating primary input signals from time-averaged isotope profiles. Geochimica et Cosmochimica Acta 69, 4101–4116.

Pasteris, J.D., Wopenka, B. and Valsami-Jones, E., 2008. Bone and tooth mineralization: Why apatite?. Elements 4, 97–104.

1063 Paul, D., Skrzypek, G., Fórizs, I., 2007. Normalization of measured stable isotopic
1064 compositions to isotope reference scales – a review. Rapid Communications
1065 in Mass Spectrometry 21, 3006–3014.
1066 Pietzner, H., Vahl, J., Werner, H., Ziegler, W., 1968. Zur chemischen
1067 zusammensetzung und mikromorphologie der conodonten. Palaeontographica
1068 Abteilung A 128, 115–152.
1069 Playford, P.E., Hocking, R.M., Cockbain, A.E., 2009. Devonian reef complexes of
1070 the Canning Basin, WA. Bulletin of the Geological Survey of Western
1071 Australia 145, 1–444.
1072 Playton, T., Montgomery, P., Tohver, E., Hillbun, K., Katz, D., Haines, P.,
1073 Trinajstic, K., Yan, M., Hansma, J., Pisarevsky, S., 2013. Development of a
1074 regional stratigraphic framework for Upper Devonian reef complexes using
1075 integrated chronostratigraphy: Lennard Shelf, Canning Basin, Western
1076 Australia, The Sedimentary Basins of Western Australia IV. Proceedings of
1077 the Petroleum Exploration Society of Australia Symposium, Perth, Western
1078 Australia.
1079 Popp, B.N., Anderson, T.F., Sandberg, P.A., 1986. Brachiopods as indicators of
1080 original isotopic compositions in some Paleozoic limestones. Geological
1081 Society of America Bulletin 97, 1262–1269.
1082 Pucéat, E., Joachimski, M.M., Bouilloux, A., Monna, F., Bonin, A., Motreuil, S.,
1083 Morinière, P., Hénard, S., Mourin, J., Dera, G., 2010. Revised phosphate -
1084 water fractionation equation reassessing paleotemperatures derived from
1085 biogenic apatite. Earth and Planetary Science Letters 298, 135–142.
1086 Pucéat, E., Lécuyer, C., Sheppard, S.M., Dromart, G., Reboulet, S., Grandjean, P.,
1087 2003. Thermal evolution of Cretaceous Tethyan marine waters inferred from

oxygen isotope composition of fish tooth enamels. Paleoceanography 18, 1–13.

Purnell, M.A., Donoghue, P.C., Aldridge, R.J., 2000. Orientation and anatomical notation in conodonts. Journal Information 74, 113–122.

Qu, Q., Haitina, T., Zhu, M., Ahlberg, P.E., 2015. New genomic and fossil data illuminate the origin of enamel. Nature 526, 108–111.

Qu, Q., Zhu, M., Wang, W., 2013. Scales and dermal skeletal histology of an early bony fish *Psarolepis romeri* and their bearing on the evolution of rhombic scales and hard tissues. PloS one 8, doi: e61485.

Quinton, P C., MacLeod, K.G., 2014. Oxygen isotopes from conodont apatite of the midcontinent, US: Implications for Late Ordovician climate evolution. Palaeogeography, Palaeoclimatology, Palaeoecology 404, 57–66.

Raoult, V., Peddemors, V.M., Zahra, D., Howell, N., Howard, D.L., de Jonge, M.D., Williamson, J.E., 2016. Strontium mineralization of shark vertebrae. Scientific Reports, 6.

Reif, W.E., 1982. Evolution of dermal skeleton and dentition in vertebrates. Evolutionary biology 15, 287–368.

Reif, W.E., 1985. Squamation and ecology of sharks. Senckenbergische Naturforschende Gesellschaft.

Reif, W., 1978. A note on the distinction between acellular bone and atubular dentine in fossil shark teeth. Neues Jahrbuch für Geologie und Paläontologie, Monatshefte 1978, 447–448.

Richter, M., Smith, M., 1995. A microstructural study of the ganoine tissue of selected lower vertebrates. Zoological Journal of the Linnean Society 114, 173–212.

1113 Richter, M., Neis, P.A., Smith, M.M., 1999. Acanthodian and actinopterygian fish
1114 remains from the Itaituba Formation, Late Carboniferous of the Amazon
1115 Basin, Brazil, with a note on acanthodian ganoin. Neues Jahrbuch für
1116 Geologie und Paläontologie, Monatshefte 1999, 728–744.
1117 Rigo, M., Trotter, J. A., Preto, N., Williams, I. S., 2012. Oxygen isotopic evidence
1118 for Late Triassic monsoonal upwelling in the northwestern Tethys,
1119 Geology, 40, 515–518.
1120 Ripa, L., Gwinnett, A., Guzman, C., Legler, D., 1972. Microstructural and
1121 microradiographic qualities of lemon shark enameloid. Archives of oral
1122 biology 17, 118–165.
1123 Roelofs, B., Barham, M., Mory, A., Trinajstic, K., 2016. Late Devonian and Early
1124 Carboniferous chondrichthyans from the Fairfield Group, Canning Basin,
1125 Western Australia. Palaeontologia Electronica 19, 1–28.
1126 Roelofs, B., Playton, T., Barham, M., Trinajstic, K., 2015. Upper Devonian
1127 microvertebrates from the Canning Basin, Western Australia. Acta Geologica
1128 Polonica 65, 69–101.
1129 Rollion-Bard, C., Saulnier, S., Vigier, N., Schumacher, A., Chaussidon, M., Lécuyer,
1130 C., 2016. Variability in magnesium, carbon and oxygen isotope compositions
1131 of brachiopod shells: Implications for paleoceanographic studies. Chemical
1132 Geology 423, 49–60.

1133 Sasagawa, I., Yokosuka, H., Ishiyama, M., Mikami, M., Shimokawa, H., Uchida, T.,
1134 2012. Fine structural and immunohistochemical detection of collar enamel in
1135 the teeth of Polypterus senegalus, an actinopterygian fish. Cell and tissue
1136 research 347, 369–381.

1137 Scharer, R.M., Patterson III, W.F., Carlson, J.K., Poulakis, G.R., 2012. Age and
1138 growth of endangered smalltooth sawfish (*Pristis pectinata*) verified with
1139 LA-ICP-MS analysis of vertebrae. PloS one 7, e47850.
1140 Schobben, M., Stebbins, A., Ghaderi, A., Strauss, H., Korn, D., Korte, C., 2015.
1141 Flourishing ocean drives the end-Permian marine mass extinction.
1142 Proceedings of the National Academy of Sciences 112, 10298–10303.
1143 Scholle, P.A., Ulmer-Scholle, D.S., 2003. A Color Guide to the Petrography of
1144 Carbonate Rocks: Grains, Textures, Porosity, Diagenesis, American
1145 Association of Petroleum Geologists Memoir 77.
1146 Schultze, H.P., 2015. Scales, Enamel, Cosmine, Ganoine, and Early
1147 Osteichthyans. Comptes Rendus Palevol 15, 83–102.
1148 Sharp, Z.D., Atudorei, V., Furrer, H., 2000. The effect of diagenesis on oxygen
1149 isotope ratios of biogenic phosphates. American Journal of Science 300, 222–
1150 237.
1151 Shemesh, A., Kolodny, Y., Luz, B., 1988. Isotope geochemistry of oxygen and
1152 carbon in phosphate and carbonate of phosphorite francolite. Geochimica et
1153 Cosmochimica Acta 52, 2565–2572.
1154 Sire, J.Y., Akimenko, M.A., 2004. Scale development in fish: a review, with
1155 description of sonic hedgehog (shh) expression in the zebrafish (*Danio rerio*).
1156 International journal of developmental biology 48, 233–248.
1157 Smith, P., Tchernov, E., 1992. Structure, Function, and Evolution of Teeth. Freund
1158 Publishing House Ltd.
1159 Stack, M.V., 1955. The chemical nature of the organic matrix of bone, dentin, and
1160 enamel. Annals of the New York Academy of Sciences 60, 585–595.

1161 Stephens, N.P., Sumner, D.Y., 2003. Famennian microbial reef facies, Napier and
1162 Oscar Ranges, Canning Basin, western Australia. Sedimentology 50, 1283–
1163 1302.
1164 Sun, Y., Joachimski, M.M., Wignall, P.B., Yan, C., Chen, Y., Jiang, H., Wang, L.,
1165 Lai, X., 2012. Lethally hot temperatures during the Early Triassic
1166 greenhouse. Science 338, 366–370.
1167 Sun, Y., Wiedenbeck, M., Joachimski, M.M., Beier, C., Kemner, F., Weinzierl, C.,
1168 2016. Chemical and oxygen isotope composition of gem-quality apatites:
1169 Implications for oxygen isotope reference materials for secondary ion mass
1170 spectrometry (SIMS). Chemical Geology 440, 164-178.
1171 Talent, J.A., Mawson, R., Andrew, A.S., Hamilton, P.J., Whitford, D.J., 1993.
1172 Middle Palaeozoic extinction events: faunal and isotopic data.
1173 Palaeogeography, Palaeoclimatology, Palaeoecology 104, 139–152.
1174 Teaford, M. F., Smith, M. M., Ferguson, M.W.J., 2000. Development, Function
1175 and Evolution of Teeth Cambridge University Press.
1176 Thomas, G., 1957. Lower Carboniferous deposits in the Fitzroy Basin, Western
1177 Australia. Australian Journal of Science 19, 160–161.
1178 Thomas, G., 1959. The Lower Carboniferous Laurel Formation of the Fitzroy Basin.
1179 Bureau of Mineral Resources Australia Report 38, 21–36.
1180 Thorrold, S.R., Campana, S.E., Jones, C.M., Swart, P.K., 1997. Factors determining
1181 $\delta^{13}C$ and $\delta^{18}O$ fractionation in aragonitic otoliths of marine fish. Geochimica
1182 et Cosmochimica Acta 61, 2909–2919.
1183 Thorson, T.B., 1971. Movement of bull sharks, *Carcharhinus leucas*, between
1184 Caribbean Sea and Lake Nicaragua demonstrated by tagging. Copeia, 336–
1185 338.

1186 Trinajstic, K., Roelofs, B., Burrow, C., Long, J., Turner, S., 2014. Devonian
1187 vertebrates from the Canning and Carnarvon Basins with an overview of
1188 Paleozoic vertebrates of Western Australia. Journal of the Royal Society of
1189 Western Australia 97, 133–151.
1190 Trotter, J.A., Fitzgerald, J.D., Kokkonen, H., Barnes, C.R., 2007. New insights into
1191 the ultrastructure, permeability, and integrity of conodont apatite determined
1192 by transmission electron microscopy. Lethaia 40, 97–110.
1193 Trotter, J.A., Williams, I.S., Barnes, C.R., Lécuyer, C., Nicoll, R.S., 2008. Did
1194 cooling oceans trigger Ordovician biodiversification? Evidence from
1195 conodont thermometry. Science 321, 550–554.
1196 Trotter, J.A., Williams, I.S., Nicora, A., Mazza, M., Rigo, M., 2015. Long-term
1197 cycles of Triassic climate change: a new $\delta^{18}O$ record from conodont apatite.
1198 Earth and Planetary Science Letters 415, 165–174.
1199 Trueman, C., Benton, M.J., Palmer, M., 2003. Geochemical taphonomy of shallow
1200 marine vertebrate assemblages. Palaeogeography, Palaeoclimatology,
1201 Palaeoecology 197, 151–169.
1202 Turner, S., 1982. Middle Palaeozoic elasmobranch remains from Australia. Journal
1203 of Vertebrate Paleontology 2, 117–131.
1204 Valiukevicus, J., Burrow, C.J., 2005. Diversity of tissues in acanthodians with
1205 *Nostolepis*-type histological structure. Acta Palaeontologica Polonica 50,
1206 635–649.
1207 Van Geldern, R., Joachimski, M., Day, J., Jansen, U., Alvarez, F., Yolkin, E., Ma,
1208 X.P., 2006. Carbon, oxygen and strontium isotope records of Devonian
1209 brachiopod shell calcite. Palaeogeography, Palaeoclimatology, Palaeoecology
1210 240, 47–67.

1211 Veizer, J., Ala, D., Azmy, K., Bruckschen, P., Buhl, D., Bruhn, F., Carden, G.A.,
1212 Diener, A., Ebneth, S., Godderis, Y., 1999. $^{87}Sr/^{86}Sr$, $\delta^{13}C$ and $\delta^{18}O$ evolution
1213 of Phanerozoic seawater. Chemical geology 161, 59–88.
1214 Veizer, J., Fritz, P., Jones, B., 1986. Geochemistry of brachiopods: oxygen and
1215 carbon isotopic records of Paleozoic oceans. Geochimica et Cosmochimica 3
1216 Acta 50, 1679–1696.
1217 Vennemann, T.W., Fricke, H.C., Blake, R.E., O'Neil, J.R., Colman, A., 2002.
1218 Oxygen isotope analysis of phosphates: a comparison of techniques for
1219 analysis of Ag_3PO_4. Chemical Geology 185, 321–336.
1220 Vennemann, T., Hegner, E., Cliff, G., Benz, G., 2001. Isotopic composition of recent
1221 shark teeth as a proxy for environmental conditions. Geochimica et
1222 Cosmochimica Acta 65, 1583–1599.
1223 Wadleigh, M.A., Veizer, J., 1992. $^{18}O/^{16}O$ and $^{13}C/^{12}C$ in lower Paleozoic articulate
1224 brachiopods: Implications for the isotopic composition of seawater.
1225 Geochimica et Cosmochimica Acta 56, 431–443.
1226 Wang, Y., Cerling, T.E., 1994. A model of fossil tooth and bone diagenesis—
1227 implications for paleodiet reconstruction from stable isotopes.
1228 Palaeogeography, Palaeoclimatolology, Palaeoecology 107, 281–289.
1229 Wenzel, B., Lécuyer, C., Joachimski, M.M., 2000. Comparing oxygen isotope
1230 records of Silurian calcite and phosphate $\delta^{18}O$ compositions of brachiopods
1231 and conodonts. Geochimica et Cosmochimica Acta 64, 1859–1872.
1232 Wheeley, J.R., Smith, M.P., Boomer, I., 2012. Oxygen isotope variability in
1233 conodonts: implications for reconstructing Palaeozoic palaeoclimates and
1234 palaeoceanography. Journal of the Geological Society 169, 239–250.

1235 Wright, E.K., Hoering, T.C., 1989. Separation and purification of phosphates for
1236 oxygen isotope analysis. Annual Report of the Director, Geophysical
1237 Laboratory, Carnegie Institute 2150, 137–141.
1238 Yamamoto, K., Asami, R., Iryu, Y., 2011. Brachiopod taxa and shell portions
1239 reliably recording past ocean environments: toward establishing a robust
1240 paleoceanographic proxy. Geophysical Research Letters 38. doi:
1241 10.1029/2011GL047134.
1242 Zaccone, G., Dabrowski, K., Hedrick, M.S., Fernandes, J.M.O., Icardo, J.M.,
1243 2015. Phylogeny, anatomy and physiology of ancient fishes. CRC Press.
1244 Zazzo, A., Lécuyer, C., Mariotti, A., 2004. Experimentally-controlled carbon and
1245 oxygen isotope exchange between bioapatites and water under inorganic and
1246 microbially-mediated conditions. Geochimica et Cosmochimica Acta 68, 1–
1247 12.
1248 Žigaitė, Ž., Joachimski, M., Lehnert, O., 2009. Oxygen Isotope Record In Biogenic
1249 Apatite: A Tool For Chemostratigraphy And Proxy In Palaeoclimate Studies,
1250 2009 Portland GSA Annual Meeting.
1251 Žigaitė, Ž., Karatajūtė-Talimaa, V., Blieck, A., 2011. Vertebrate microremains from
1252 the Lower Silurian of Siberia and Central Asia: palaeobiodiversity and
1253 palaeobiogeography. Journal of Micropalaeontology 30, 97–106.
1254 Žigaitė, Ž., Whitehouse, M., 2014. Stable oxygen isotopes of dental biomineral:
1255 differentiation at the intra-and inter-tissue level of modern shark teeth. GFF
1256 136, 337–340.
1257 Žigaitė, Ž., Fadel, A., Blom, H., Perez-Huerta, A., Jeffries, T., Märss, T., Ahlberg, P.
1258 E., 2015. Rare earth elements (REEs) in vertebrate microremains from the

upper Pridoli Ohesaare beds of Saaremaa Island, Estonia: geochemical clues to palaeoenvironment. Estonian Journal of Earth Sciences, 64, 115–120.

Fig. 1. Regional geology map and sampled sites from the Lennard Shelf, Canning Basin, Western Australia (modified from Playford et al., 2009).

Fig. 2. Frasnian *Palmatolepis* P-elements. (**A**) Back-scattered electron microscope image in aboral view with x4 magnified inset (i) highlighting the well-preserved ornamentation. (**B**) Stereo microscope image of a polished *Palmatolepis* sp. element showing the well-preserved internal microstructures and low Colour Alteration Index (CAI).

Fig. 3. Gas Isotope Ratio Mass Spectrometry (GIRMS) analyses of vertebrate microfossil elements from the late Famennian (i) and early Tournaisian (ii). Data points give average value of replicate analyses, vertical bars represent 1 std.dev. Coeval conodont values obtained from SIMS (late Famennian = +19.6 ±0.5 ‰ and; early Tournaisian = +20.3 ±0.8 ‰) were generally higher than vertebrate microfossil values analysed by GIRMS.

Fig. 4. Secondary Ion Mass Spectrometry (SIMS) $\delta^{18}O$ analyses of vertebrate microfossil elements from the late Famennian (i) and early Tournaisian (ii). Data points are the averages of spot clusters with 1 std.dev. given by the vertical error bars. Average vertebrate microfossil $\delta^{18}O$ values are plotted as difference relative to the $\delta^{18}O$ of co-occurring conodonts to focus on the tissue-specific differences

1284 regardless of geological age. Conodont $\delta^{18}O$ values were obtained from secondary
1285 ion mass spectrometry (SIMS) ($\delta^{18}O_{conodont}$ values for the late Famennian = +19.6
1286 ±0.5 ‰ and; early Tournaisian = +20.3 ±0.8 ‰). Grey area represents 1 std.dev. of
1287 average co-occurring $\delta^{18}O_{conodont}$ obtained by SIMS.
1288
1289 **Fig. 5**. $\delta^{18}O$ of tissue types from two early Tournaisian Holocephalan teeth compared
1290 to average $\delta^{18}O$ of coeval conodonts (+20.3 ±0.8 ‰). (A) Tooth (MTM1-H1)
1291 showing analysis of enameloid and dentine tissues; (A) Analysis of a tooth (MTM1-
1292 H9) showing variation in $\delta^{18}O$ values associated with exposure of the labial surface
1293 (indicated by dashed line). Coloured boxes correspond to spot clusters depicted in
1294 the graphs A, B. Grey area represents 1 std.dev. (±0.8 ‰) of the average $\delta^{18}O$ of
1295 associated conodonts analysed by SIMS. For (B) spot numbers 1-3, 5-7 and 14-16
1296 represent surface enameloid with pore enamel represented by spot numbers 4, 11-13
1297 and 17-18.
1298
1299 **Fig. 6**. Systematic $\delta^{18}O$ variation in early Tournaisian vertebrate microfossil tissues
1300 analysed via SIMS. Location of ion-probe spots indicated on stereo-microscope
1301 images of polished analytical surface. (A) Palaeoniscoid fish tooth (MT-4 PN) with
1302 acrodin cap and dentine tissue analysed; (B) Analysis of enameloid and dentine
1303 tissues from Protacrodont tooth (1984-04 Dh2), referred to as *Dalmehodus* cf.
1304 *turnerae* (Roelofs et al., 2016); (c) Tooth of the chondrichthyan *Ageleodus* (1984-04
1305 AG1) showing a transect of spot analyses from the cusp apex to the base. All values
1306 plotted relative to a co-occurring conodont $\delta^{18}O$ value of +20.3 ±0.8 ‰. Grey areas
1307 in graphs represent 1 std. dev. (±0.8 ‰) of $\delta^{18}O$ analyses of co-occurring conodonts.
1308

Fig. 7. Comparison of GIRMS and tissue specific targeting via SIMS analysis on individual fossil elements from the (i) Famennian (average conodont $\delta^{18}O$ value of +19.6 ±0.5 ‰ from three elements) and (ii) Tournaisian (average conodont $\delta^{18}O$ value of +20.3 ±0.8 ‰ from two elements). Grey area in the graph represents 1 std.dev. of $\delta^{18}O$ analyses of co-occurring conodonts.

Table 1

Late Famennian and early Tournaisian vertebrate microfossils and standards analysed using gas isotope ratio mass spectrometry (GIRMS).

[a] Number of replicate analysis

[b] Frasnian

[c] Famennian

[d] Tournaisian

Table 2

$\delta^{18}O$ values of Durango apatite and late Famennian to early Tournaisian vertebrate microfossils analysed using SIMS.

[a] Number of replicate analysis

[b] Frasnian

[c] Famennian

[d] Tournaisian

[e] Enameloid

[f] i and ii notation indicate different individual fossils

Figure 1

Click here to download high resolution image

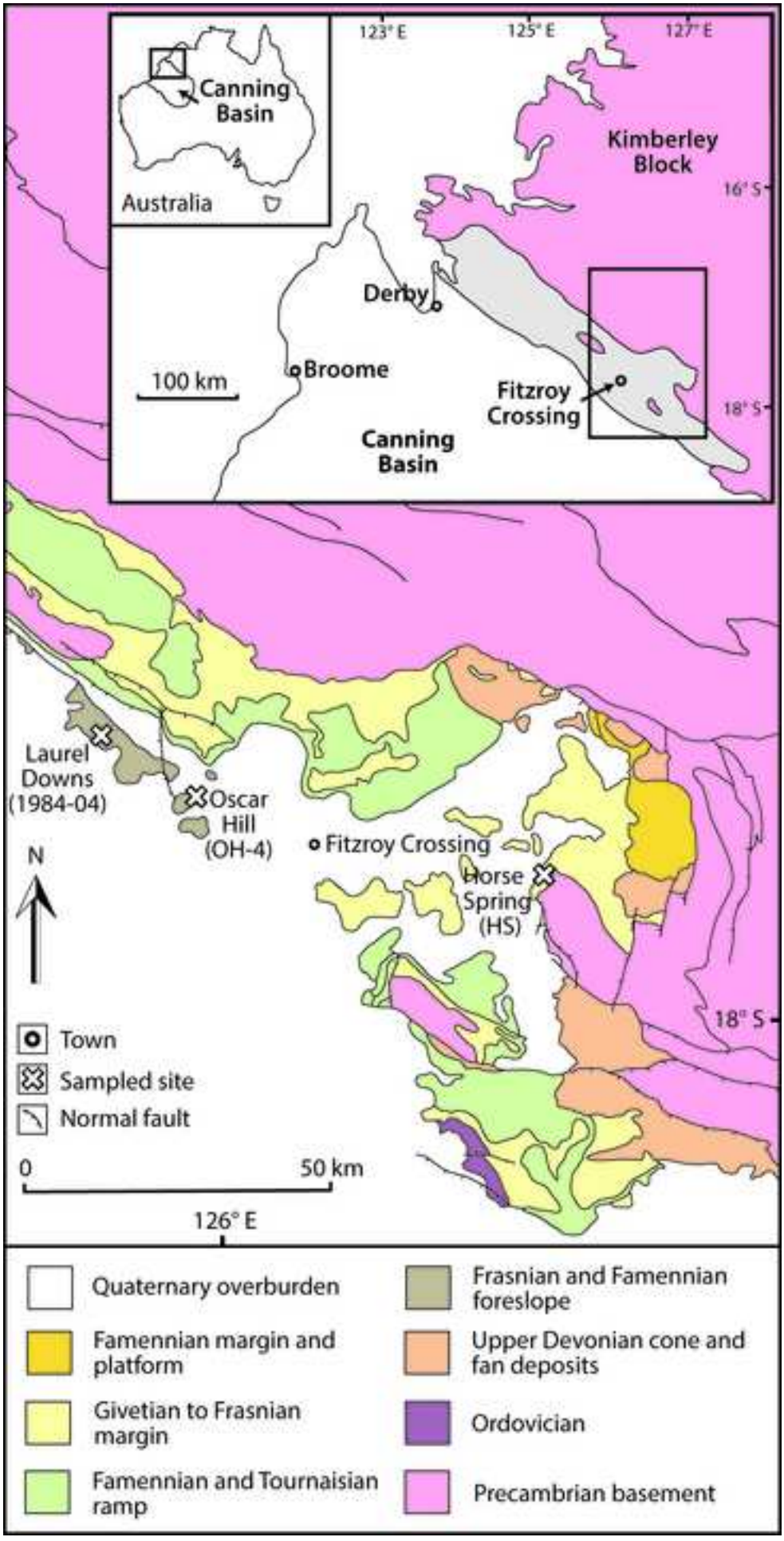

Figure 1 Caption

Fig. 1. Regional geology map and sampled sites from the Lennard Shelf, Canning Basin, Western Australia (modified from Playford et al., 2009).

Figure 2

Click here to download high resolution image

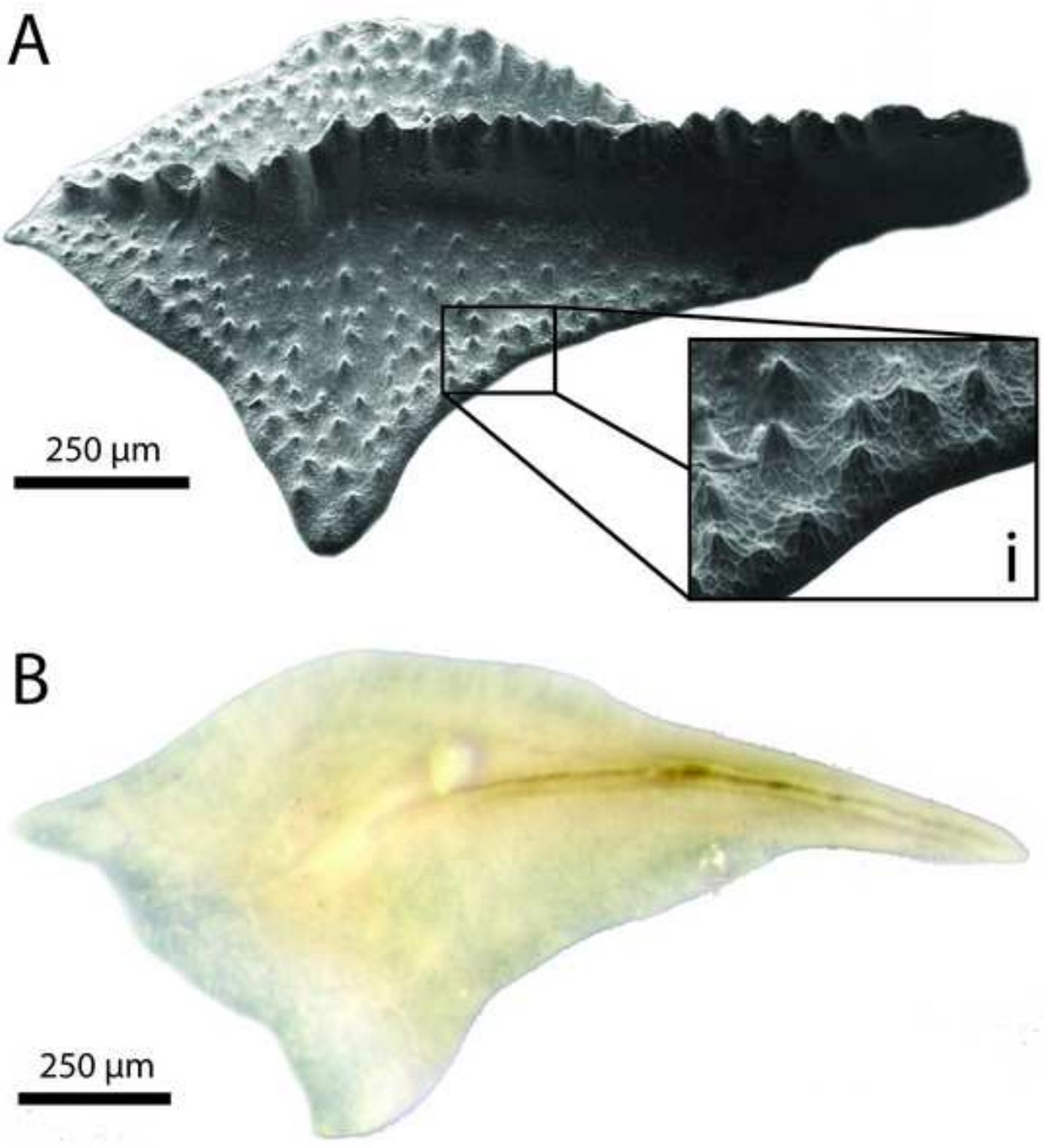

Figure 2 Caption

Fig. 2. Frasnian *Palmatolepis* P-elements. (**A**) Back-scattered electron microscope image in aboral view with x4 magnified inset (i) highlighting the well-preserved ornamentation. (**B**) Stereo microscope image of a polished *Palmatolepis* sp. element showing the well-preserved internal microstructures and low Colour Alteration Index (CAI).

Figure 3

Click here to download high resolution image

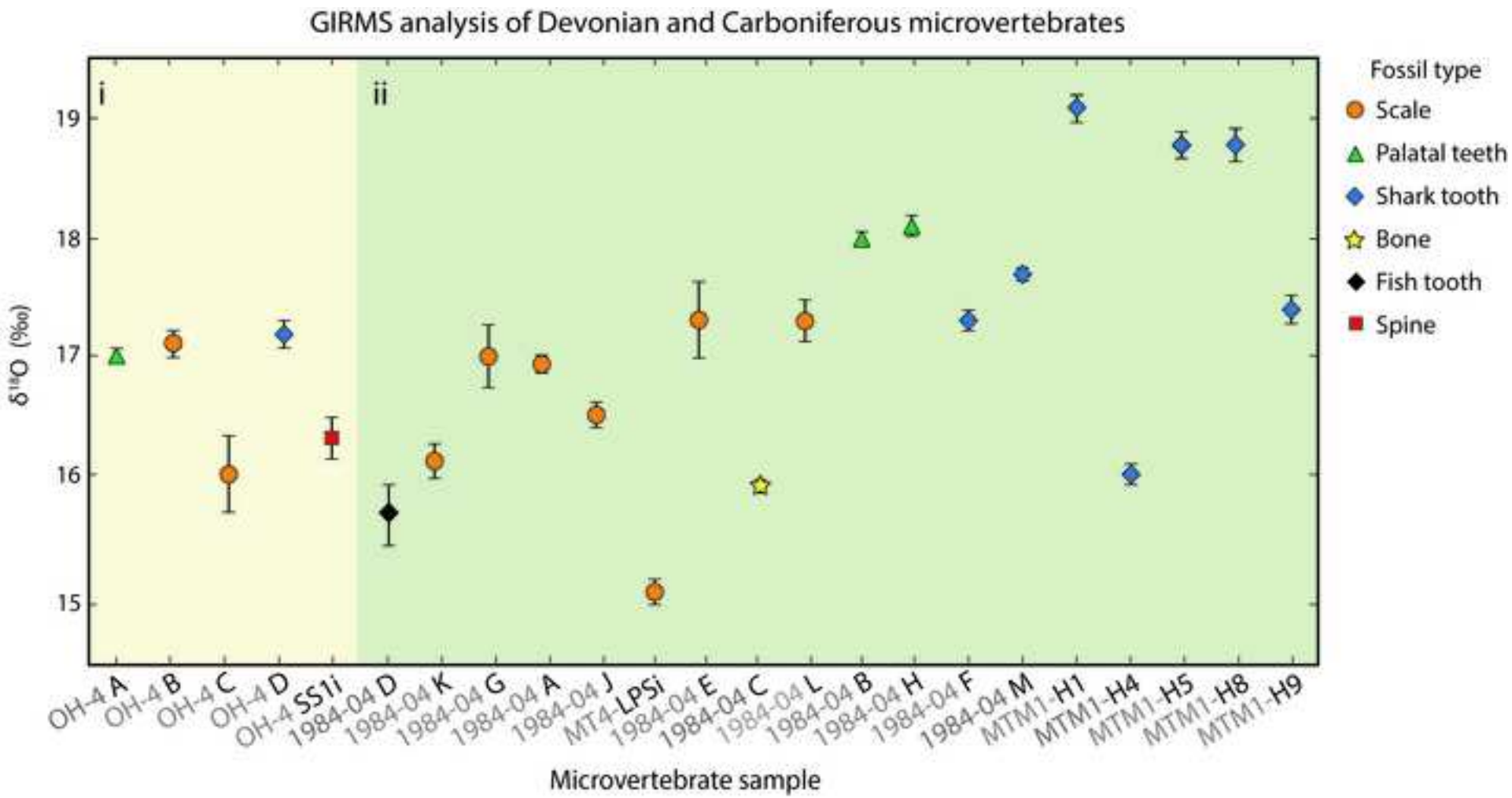

Figure 3 Caption

Fig. 3. Gas Isotope Ratio Mass Spectrometry (GIRMS) analyses of vertebrate microfossil elements from the late Famennian (i) and early Tournaisian (ii). Data points give average value of replicate analyses, vertical bars represent 1 std.dev. Coeval conodont values obtained from SIMS (late Famennian = +19.6 ±0.5 ‰ and; early Tournaisian = +20.3 ±0.8 ‰) were generally higher than vertebrate microfossil values analysed by GIRMS.

Figure 4

Click here to download high resolution image

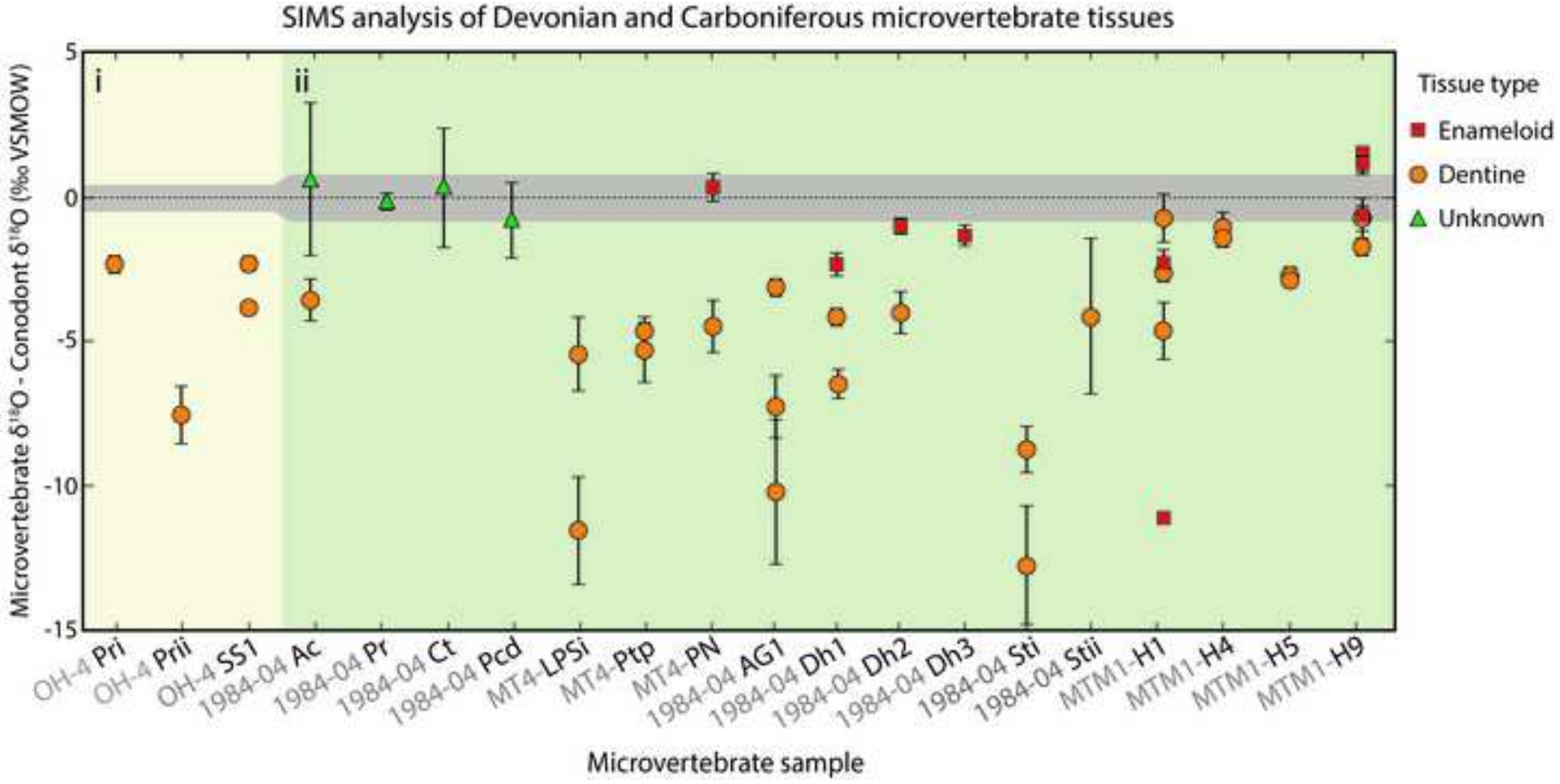

Figure 4 Caption

Fig. 4. Secondary Ion Mass Spectrometry (SIMS) $\delta^{18}O$ analyses of vertebrate microfossil elements from the late Famennian (i) and early Tournaisian (ii). Data points are the averages of spot clusters with 1 std.dev. given by the vertical error bars. Average vertebrate microfossil $\delta^{18}O$ values are plotted as difference relative to the $\delta^{18}O$ of co-occurring conodonts to focus on the tissue-specific differences regardless of geological age. Conodont $\delta^{18}O$ values were obtained from secondary ion mass spectrometry (SIMS) ($\delta^{18}O_{conodont}$ values for the late Famennian = +19.6 ±0.5 ‰ and; early Tournaisian = +20.3 ±0.8 ‰). Grey area represents 1 std.dev. of average co-occurring $\delta^{18}O_{conodont}$ obtained by SIMS.

Figure 5

Click here to download high resolution image

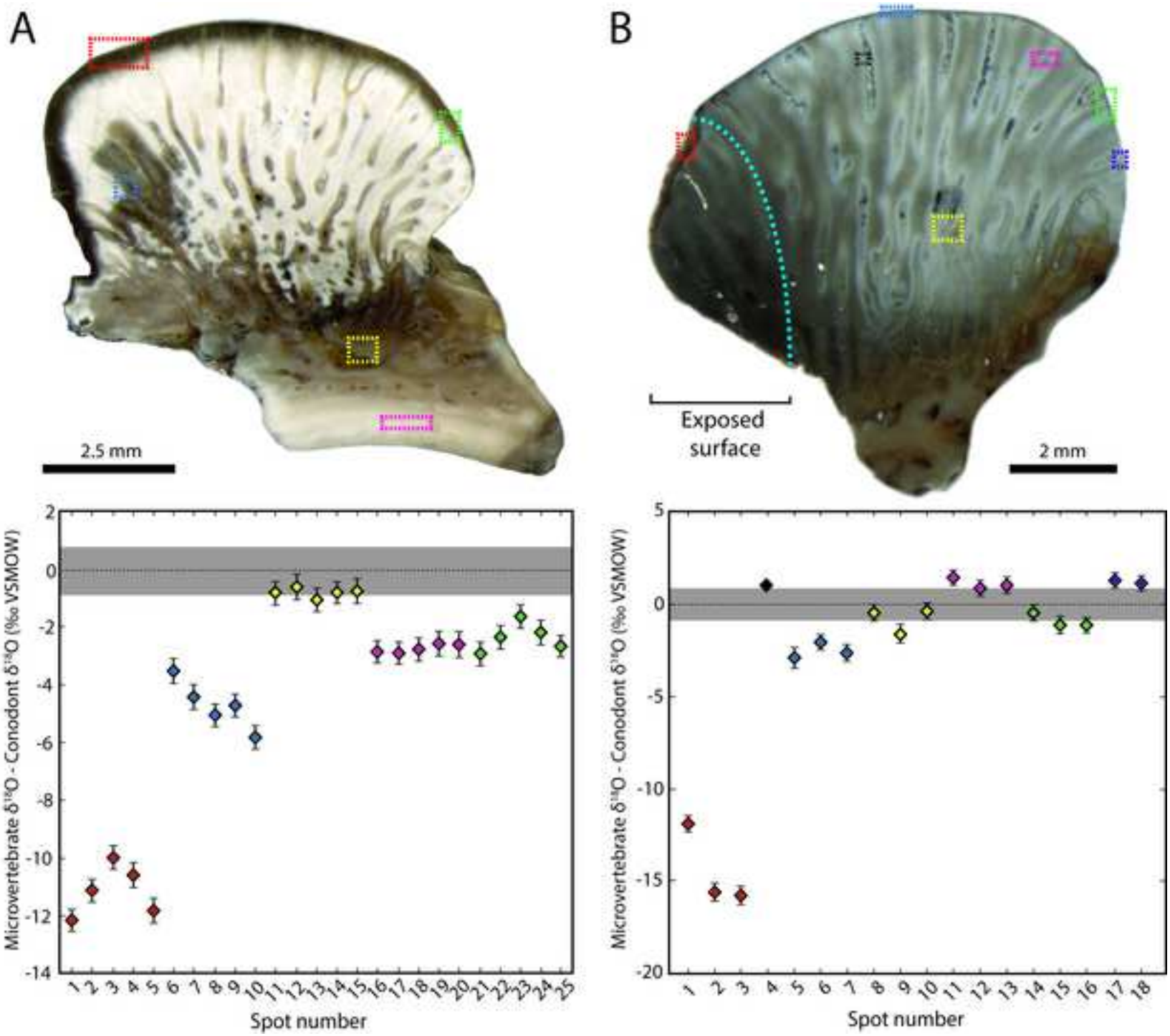

Figure 5 Caption

Fig. 5. $\delta^{18}O$ of tissue types from two early Tournaisian Holocephalan teeth compared to average $\delta^{18}O$ of coeval conodonts (+20.3 ±0.8 ‰). (A) Tooth (MTM1-H1) showing analysis of enameloid and dentine tissues; (A) Analysis of a tooth (MTM1-H9) showing variation in $\delta^{18}O$ values associated with exposure of the labial surface (indicated by dashed line). Coloured boxes correspond to spot clusters depicted in the graphs A, B. Grey area represents 1 std.dev. (±0.8 ‰) of the average $\delta^{18}O$ of associated conodonts analysed by SIMS. For (B) spot numbers 1-3, 5-7 and 14-16 represent surface enameloid with pore enamel represented by spot numbers 4, 11-13 and 17-18.

Figure 6

Click here to download high resolution image

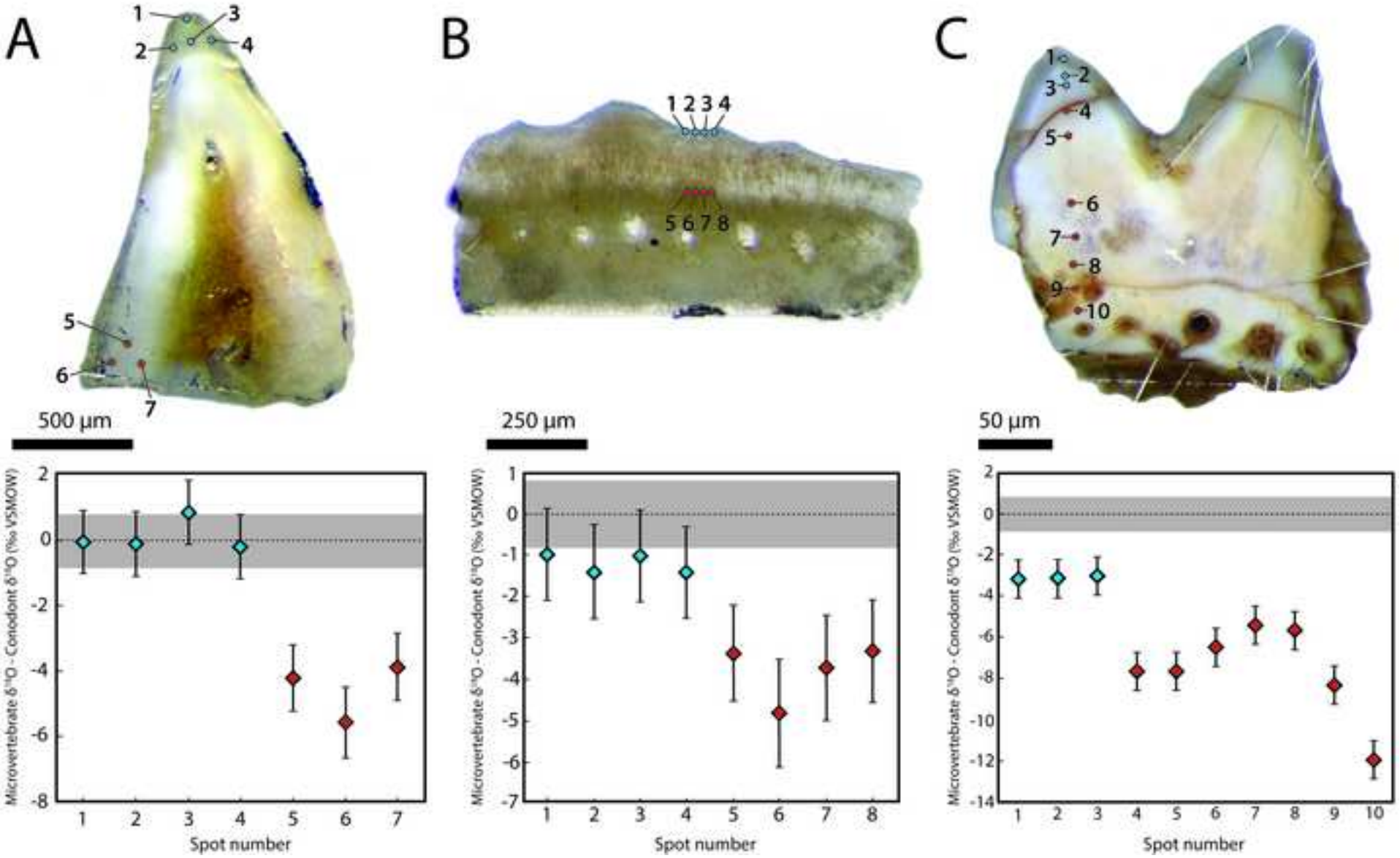

Figure 6 Caption

Fig. 6. Systematic $\delta^{18}O$ variation in early Tournaisian vertebrate microfossil tissues analysed via SIMS. Location of ion-probe spots indicated on stereo-microscope images of polished analytical surface. (A) Palaeoniscoid fish tooth (MT-4 PN) with acrodin cap and dentine tissue analysed; (B) Analysis of enameloid and dentine tissues from Protacrodont tooth (1984-04 Dh2), referred to as *Dalmehodus* cf. *turnerae* (Roelofs et al., 2016); (c) Tooth of the chondrichthyan *Ageleodus* (1984-04 AG1) showing a transect of spot analyses from the cusp apex to the base. All values plotted relative to a co-occurring conodont $\delta^{18}O$ value of +20.3 ±0.8 ‰. Grey areas in graphs represent 1 std. dev. (±0.8 ‰) of $\delta^{18}O$ analyses of co-occurring conodonts.

Figure 7

Click here to download high resolution image

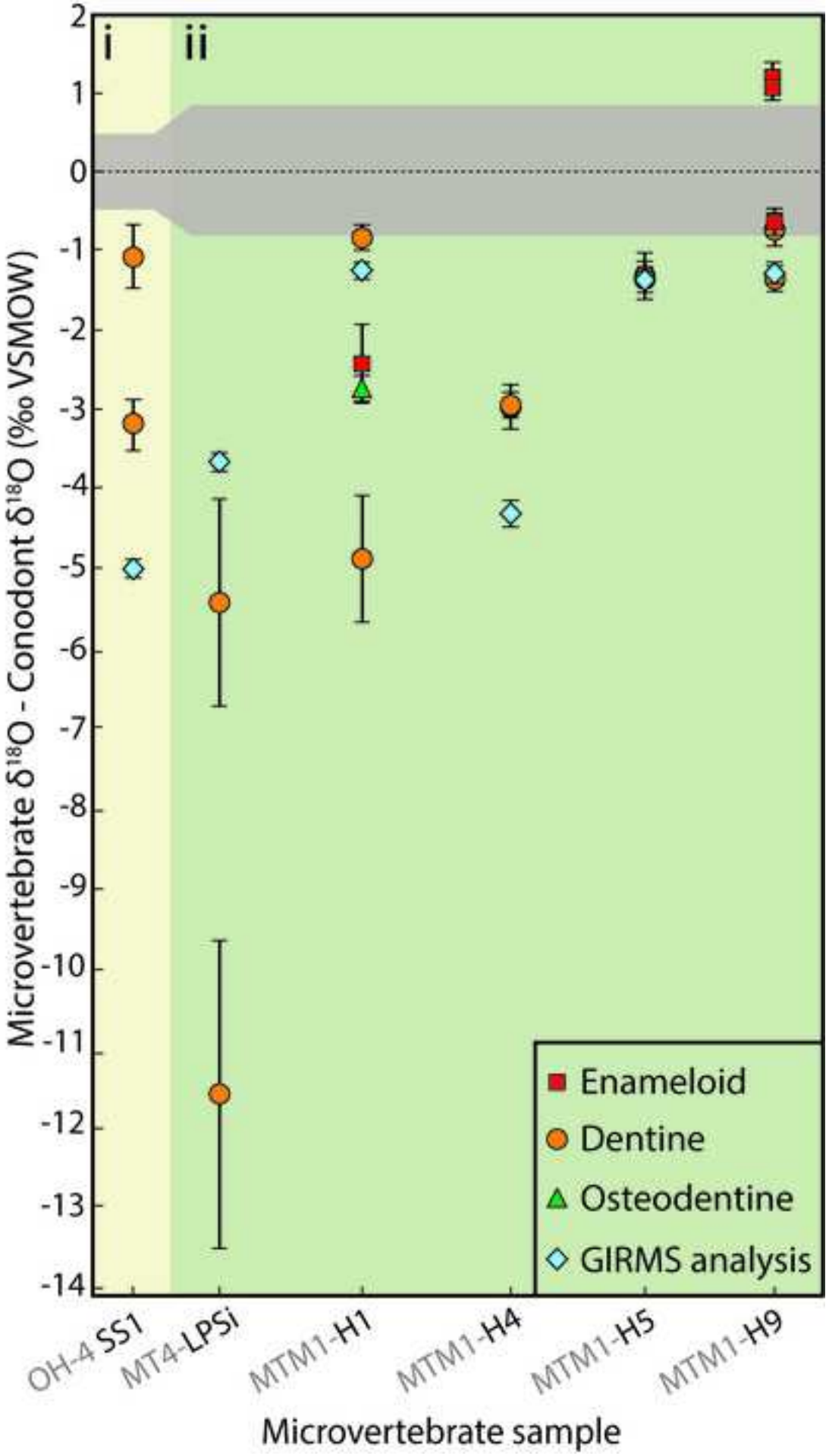

Figure 7 Caption

Fig. 7. Comparison of GIRMS and tissue specific targeting via SIMS analysis on individual vertebrate microfossil elements from the (i) Famennian (average conodont $\delta^{18}O$ value of +19.6 ±0.5 ‰ from three elements) and (ii) Tournaisian (average conodont $\delta^{18}O$ value of +20.3 ±0.8 ‰ from two elements). Grey area in the graph represents 1 std.dev. of $\delta^{18}O$ analyses of co-occurring conodonts.

Table 1

Late Famennian and early Tournaisian vertebrate microfossils and standards analysed using gas isotope ratio mass spectrometry (GIRMS).

Location	Sample no.	Formation (Fm.)	Age	Sample	Taxa	Sample size (mg)	n[a]	$\delta^{18}O$ (‰)	1σ
Horse Spring	VHS-312	Virgin Hills Fm.	Fr[b]	*Ancyrodella*	Conodont	0.88	3	19.0	0.2
Oscar Hill	OH-4 A	Gumhole Fm.	Fn[c]	Palatal teeth	Palaeoniscoid	0.99	3	17.0	0.1
Oscar Hill	OH-4 B	Gumhole Fm.	Fn[c]	Scale	Protacrodont	2.04	3	17.1	0.2
Oscar Hill	OH-4 C	Gumhole Fm.	Fn[c]	Scale	Ctenacanthid	0.60	2	16.0	0.6
Oscar Hill	OH-4 D	Gumhole Fm.	Fn[c]	Tooth cusp	*Helodus*	0.89	3	17.2	0.3
Oscar Hill	OH4-SS1	Gumhole Fm.	Fn[c]	Spine	Shark	-	3	16.3	0.1
Laurel Downs	1984-04 A	Laurel Fm.	Tn[d]	Scale	Ctenacanthid	1.25	3	16.9	0.1
Laurel Downs	1984-04 B	Laurel Fm.	Tn[d]	Palatal teeth	Palaeoniscoid	0.82	3	18.0	0.2
Laurel Downs	1984-04 C	Laurel Fm.	Tn[d]	Radial bone	Palaeoniscoid	0.70	1	15.9	0.1
Laurel Downs	1984-04 D	Laurel Fm.	Tn[d]	Teeth	Palaeoniscoid	0.85	3	15.7	0.5
Laurel Downs	1984-04 E	Laurel Fm.	Tn[d]	Scale	Palaeoniscoid	1.51	3	17.3	0.6
Laurel Downs	1984-04 F	Laurel Fm.	Tn[d]	Tooth cusp	Holocephalan	1.63	3	17.3	0.2
Laurel Downs	1984-04 M	Laurel Fm.	Tn[d]	Tooth cusp	Holocephalan	0.87	3	17.7	0.1
Laurel Downs	1984-04 G	Laurel Fm.	Tn[d]	Scales	Acanthodian	0.77	3	17	0.4
Laurel Downs	1984-04 H	Laurel Fm.	Tn[d]	Palatal teeth	Palaeoniscoid	1.42	3	18.1	0.4
Laurel Downs	1984-04 J	Laurel Fm.	Tn[d]	Scale	Lungfish	1.44	3	16.5	0.2
Laurel Downs	1984-04 K	Laurel Fm.	Tn[d]	Scale	Protacrodont	1.13	3	16.1	0.3
Laurel Downs	1984-04 L	Laurel Fm.	Tn[d]	Scale	Protacrodont	0.96	3	17.3	0.5
Laurel Downs	MTM1-H1	Laurel Fm.	Tn[d]	Tooth cusp	Holocephalan	-	3	19.1	0.1
Laurel Downs	MTM1-H4	Laurel Fm.	Tn[d]	Tooth cusp	Holocephalan	-	3	16	0.2
Laurel Downs	MTM1-H5	Laurel Fm.	Tn[d]	Tooth cusp	Holocephalan	-	3	18.8	0.2
Laurel Downs	MTM1-H8	Laurel Fm.	Tn[d]	Tooth cusp	Holocephalan	-	3	18.8	0.1
Laurel Downs	MTM1-H9	Laurel Fm.	Tn[d]	Tooth cusp	Holocephalan	-	3	17.4	0.3
Laurel Downs	MT4-LPS	Laurel Fm.	Tn[d]	Scale	Lungfish	-	3	15.1	0.0

[a] Number of replicate analysis

[b] Frasnian

[c] Famennian

[d] Tournaisian

Table 1

Late Famennian and early Tournaisian vertebrate microfossils and standards analysed using gas isotope ratio mass spectrometry (GIRMS).

[a] Number of replicate analysis

[b] Frasnian

[c] Famennian

[d] Tournaisian

Table 2

$\delta^{18}O$ values of Durango apatite and late Famennian to early Tournaisian microfossils analysed using SIMS.

Location	Sample no.	Formation (Fm.)	Age	Sample	Taxa	Tissue	n[a]	$\delta^{18}O$ (‰)	1σ
Horse Spring	VHS-312a	Virgin Hills Fm.	Fr[b]	P-element	*Palmatolepis*	Hyaline	4	19.1	0.3
Horse Spring	VHS-312b	Virgin Hills Fm.	Fr[b]	P-element	*Ancyrodella*	Hyaline	4	19.2	0.3
Oscar Hill	OH4-CS2	Gumhole Fm.	Fn[c]	S-element	Conodont	Hyaline	5	19.9	0.5
Oscar Hill	Si-OH4i[f]	Gumhole Fm.	Fn[c]	S-element	Conodont	Hyaline	2	20.1	1
Oscar Hill	Si-OH4ii[f]	Gumhole Fm.	Fn[c]	S-element	Conodont	Hyaline	2	18.8	0
Oscar Hill	OH4-SS1	Gumhole Fm.	Fn[c]	Shark spine	Unknown	Dentine	4	16.5	0.4
Oscar Hill	OH4-SS1	Gumhole Fm.	Fn[c]	Shark Spine	Unknown	Dentine	3	18.5	0.3
Oscar Hill	OH4-Pri	Gumhole Fm.	Fn[c]	Scale	Protacrodont	Unknown	2	17.9	0.1
Oscar Hill	OH4-Prii	Gumhole Fm.	Fn[c]	Scale	Protacrodont	Unknown	2	12.8	1
Laurel Downs	CCA1	Laurel Fm.	Tn[d]	P-element	*Clydagnathus*	Hyaline	5	20.9	.9
Laurel Downs	CCA2	Laurel Fm.	Tn[d]	P-element	*Clydagnathus*	Hyaline	4	19.9	0.4
Laurel Downs	1984-04 Ac	Laurel Fm.	Tn[d]	Scale	Acanthodian	Unknown	2	20.6	1.6
Laurel Downs	1984-04 Ac	Laurel Fm.	Tn[d]	Scale	Acanthodian	Dentine	1	16.7	n/a
Laurel Downs	1984-04 Pr	Laurel Fm.	Tn[d]	Scale	Protacrodont	Unknown	3	20.1	0.3
Laurel Downs	1984-04 Ct	Laurel Fm.	Tn[d]	Scale	Ctenacanthid	Unknown	2	20.6	2.1
Laurel Downs	1984-04 Pcd	Laurel Fm.	Tn[d]	Scale	Palaeoniscoid	Unknown	2	19.5	1.3
Laurel Downs	MT4-LPSi[f]	Laurel Fm.	Tn[d]	Scale	Lungfish	Unknown	3	8.8	1.9
Laurel Downs	MT4-LPSi[f]	Laurel Fm.	Tn[d]	Scale	Lungfish	Unknown	5	14.9	1.3
Laurel Downs	MT4 Ptp	Laurel Fm.	Tn[d]	Palatal teeth	Palaeoniscoid	Cusp	4	15.7	0.5
Laurel Downs	MT4 Ptp	Laurel Fm.	Tn[d]	Palatal teeth	Palaeoniscoid	Dentine	4	14.9	1.1
Laurel Downs	Mt-4 PN	Laurel Fm.	Tn[d]	Tooth	Palaeoniscoid	Acrodin	4	20.7	0.5
Laurel Downs	Mt-4 PN	Laurel Fm.	Tn[d]	Tooth	Palaeoniscoid	Dentine	3	15.9	0.9
Laurel Downs	1984-04 AG1	Laurel Fm.	Tn[d]	Tooth	*Ageleodus* sp.	Dentine	3	17.2	0.1
Laurel Downs	1984-04 AG1	Laurel Fm.	Tn[d]	Tooth	*Ageleodus* sp.	Dentine	5	13.1	1.1
Laurel Downs	1984-04 AG1	Laurel Fm.	Tn[d]	Tooth	*Ageleodus* sp.	Dentine	2	10.1	2.5
Laurel Downs	1984-04 Dh1	Laurel Fm.	Tn[d]	Tooth	Protacrodont	Enameloid	3	17.9	0.4
Laurel Downs	1984-04 Dh1	Laurel Fm.	Tn[d]	Tooth	Protacrodont	Dentine	3	16.2	0.2
Laurel Downs	1984-04 Dh1	Laurel Fm.	Tn[d]	Tooth	Protacrodont	Dentine	3	13.8	0.5
Laurel Downs	1984-04 Dh2	Laurel Fm.	Tn[d]	Tooth	Protacrodont	Enameloid	4	19.2	0.2
Laurel Downs	1984-04 Dh2	Laurel Fm.	Tn[d]	Tooth	Protacrodont	Dentine	4	16.4	0.7
Laurel Downs	1984-04 Dh3	Laurel Fm.	Tn[d]	Tooth	Protacrodont	Enameloid	3	18.9	0.3
Laurel Downs	1984-04 Sti[f]	Laurel Fm.	Tn[d]	Tooth	Cladodont	Dentine	4	7.5	2.1
Laurel Downs	1984-04 Sti[f]	Laurel Fm.	Tn[d]	Tooth	Cladodont	Dentine	4	11.5	0.8
Laurel Downs	1984-04 Stii[f]	Laurel Fm.	Tn[d]	Tooth	Cladodont	Dentine	4	16.1	2.7
Laurel Downs	MTM1-H1	Laurel Fm.	Tn[d]	Tooth	Holocephalan	Surface en[d]	5	18.1	0.5
Laurel Downs	MTM1-H1	Laurel Fm.	Tn[d]	Tooth	Holocephalan	Surface en[d]	5	9.2	0.9
Laurel Downs	MTM1-H1	Laurel Fm.	Tn[d]	Tooth	Holocephalan	Dentine	5	19.5	0.2
Laurel Downs	MTM1-H1	Laurel Fm.	Tn[d]	Tooth	Holocephalan	Dentine	5	15.6	0.8
Laurel Downs	MTM1-H1	Laurel Fm.	Tn[d]	Tooth	Holocephalan	Dentine	5	17.6	0.1
Laurel Downs	MTM1-H4	Laurel Fm.	Tn[d]	Tooth	Holocephalan	Dentine	4	18.7	0.1
Laurel Downs	MTM1-H4	Laurel Fm.	Tn[d]	Tooth	Holocephalan	Dentine	4	19.2	0.4
Laurel Downs	MTM1-H5	Laurel Fm.	Tn[d]	Tooth	Holocephalan	Dentine	4	17.3	0.2
Laurel Downs	MTM1-H5	Laurel Fm.	Tn[d]	Tooth	Holocephalan	Dentine	4	17.3	0.3

Laurel Downs	MTM1-H9	Laurel Fm.	Tn[d]	Tooth	Holocephalan	Surface en[e]	3	5.9	2.2
Laurel Downs	MTM1-H9	Laurel Fm.	Tn[d]	Tooth	Holocephalan	Pore en[e]	3	21.4	0.3
Laurel Downs	MTM1-H9	Laurel Fm.	Tn[d]	Tooth	Holocephalan	Surface en[e]	3	17.8	0.4
Laurel Downs	MTM1-H9	Laurel Fm.	Tn[d]	Tooth	Holocephalan	Pore en[e]	2	21.8	0.1
Laurel Downs	MTM1-H9	Laurel Fm.	Tn[d]	Tooth	Holocephalan	Pore en[e]	1	21.4	n/a
Laurel Downs	MTM1-H9	Laurel Fm.	Tn[d]	Tooth	Holocephalan	Surface en[e]	3	19.5	0.7
Laurel Downs	MTM1-H9	Laurel Fm.	Tn[d]	Tooth	Holocephalan	Dentine	3	17.2	0.4

[a] Number of replicate analysis

[b] Frasnian

[c] Famennian

[d] Tournaisian

[e] Enameloid

[f] i and ii notation indicate different individual fossils

Table 2

$\delta^{18}O$ values of Durango apatite and late Famennian to early Tournaisian vertebrate microfossils analysed using SIMS.

[a] Number of replicate analysis

[b] Frasnian

[c] Famennian

[d] Tournaisian

[e] Enameloid

[f] i and ii notation indicate different individual fossils